Vibration Cancellation Using Synthetic Shunt Impedances

S.S. Groothuis, R.J. Roesthuis

MSc. Internship Thesis
February 2010

Supervisors:
A/Prof. K. Sammut
A/Prof. F. He

Abstract

The goal of this project was to achieve vibration control for a mechanical structure using shunt control and synthetic impedances. To that end a mechanical isolation system was designed and realised. The system consists of a base plate and a top plate between which three electromagnetic transducers are placed. A disturbance is applied to the base by applying a disturbance signal to an electromagnetic transducer which is also placed on the base plate. This disturbance transducer causes the base to vibrate and this vibration is then coupled into the top plate. The goal was then to reduce vibrations in the top plate using vibration control.

Vibration control of the top plate was achieved by connecting shunt circuits to the terminals of the three control transducers. These shunt circuits consist of impedances which were realised digitally using Simulink and dSpace, hence the name synthetic impedance. These impedances were designed such that reduction of vibration was achieved for a single mode of vibration at a frequency of 26.9 Hz.

Two different types of controllers were designed and realised: a resistor-capacitor controller (RC-controller) and a resistor-inductor-capacitor controller (RLC-controller). With the RC-controller a maximum reduction in top plate velocity of 11.8 dB was achieved. With the RLC-controller a maximum reduction of 16.4 dB was achieved.

Acknowledgments

This internship would not have been possible without the help of a number of people. The authors would like to thank A/Prof. Karl Sammut and A/Prof. Fangpo He for their supervision and valuable input to this project. Also, Richard Stanley, Damian Kleiss, Craig Dawson and Joel Cottrel are thanked for their much appreciated help in the mechanical and electronics workshops.

Also the following people are thanked for their help and support during and in the preparation of this internship at Flinders University: Dr. Maarten Korsten, Belinda Jaarsma-Knol, Dr. Ir. Theo de Vries, Christian van der Horst and the student support staff. Of course, our families are also thanked for supporting us in going to Australia.

Contents

1

Introduction

When a mechanical system is subject to an oscillatory motion, this is often referred to as vibration. All mechanical structures will experience vibration in some sort of way because of environmental conditions or dynamic loading. Sometimes these vibrations are desired, such as in the case of a guitar string. But often these vibrations are undesired. When one is working with sensitive measuring equipment, vibrations can cause errors in the measurement. Another example of undesired vibrations can be found in structures such as bridges. In time these vibrations can cause metal fatigue and eventually the entire structure can fail. In case of undesired vibrations, one is interested in reducing these vibrations. Vibration control then proves to be a valuable tool in reducing vibrations in all sorts of applications.

1.1 Vibration Isolation

Reduction of vibration can be achieved in a number of ways. The most common are stiffening, damping and isolation. In stiffening the stiffness of the mechanical structure is increased and this causes the resonance frequency to increase. One is then able to shift the resonance frequency beyond the frequency band of excitation. In damping the vibration energy is dissipated. This can be done passively by adding a mechanical damper or electrically by converting the mechanical energy into electrical energy and dissipating this in an electrical network. Another method of reducing the vibration is by vibration isolation. The goal of vibration isolation is to prevent vibrations from propagating into certain parts of the system. An example of vibration isolation is a table with sensitive equipment inside an ambulance. Irregularities in the road surface will cause vibrations to propagate from the chassis into the table in the ambulance. This situation is shown in Figure 1.1a: mass m represents the table and y represents the chassis displacement. The vibrations propagating into the table are undesired and vibration isolation can be used to reduce these vibrations (see Figure 1.1b).

The transmissibility $T(s)$ is defined as the transfer function from the base displacement $y(s)$ to the mass displacement $x(s)$

$$T(s) = \frac{x(s)}{y(s)} = \frac{ds + k}{ms^2 + ds + k} = \frac{2\zeta\omega_n s + \omega_n^2}{s^2 + 2\zeta\omega_n s + \omega_n^2} \tag{1.1}$$

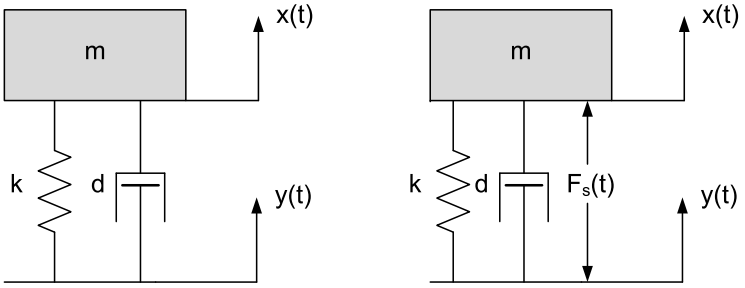

(a) Table subjected to a support excitation.

(b) Vibration isolation system.

Figure 1.1: Example of a system where vibration isolation can be useful.

With ζ being the damping ratio which is defined as

$$\zeta = \frac{d}{2\omega_n m} \tag{1.2}$$

The transmissibility is plotted for different values of the damping ratio in Figure 1.2. In vibration isolation it is desired to have a large reduction in the resonance peak and high attenuation at high frequencies. As is shown in Figure 1.2, large damping is required to reduce the resonant peak. However, this has a negative effect on the attenuation at high frequencies. This means a trade-off has to be made between resonance peak reduction and high-frequency attenuation.

1.2 Shunt Control

In shunt control, an electrical impedance is connected to the terminals of a transducer. Mechanical energy is transformed into electrical energy by the transducer. By connecting the impedance to the transducers terminals, the electrical energy is dissipated and a reduction of vibration can be achieved. The transducer used in this thesis is an electromagnetic transducer: a so called car shaker used in car audio systems.

Shunt control has a number of advantages compared to active feedback control. In the first place shunt control is cheaper because it does not require additional sensors. Secondly, collocation is guaranteed because actuation and sensing is done at the same location. In certain controller classes, collocation achieves closed-loop stability, robustness and reduces the complexity of the design process [1].

1.3 Thesis Outline

In this thesis electromagnetic shunt control was used to reduce vibrations in a plate which is supported by a vibrating structure (see Figure 1.1b). An analogy can be drawn with the table in the ambulance: the plate is comparable to

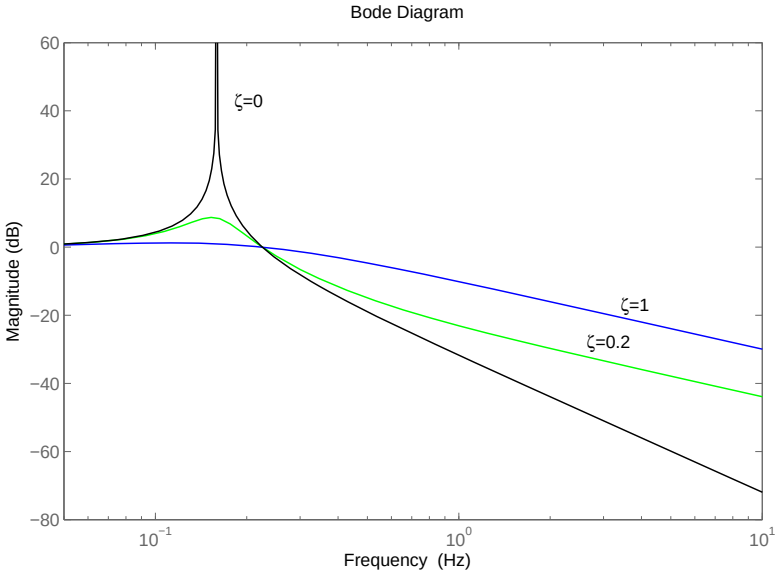

Figure 1.2: Transmissibility $T(s)$ plotted for different values of the damping ratio ζ

the table and the supporting structure is comparable with the chassis of the ambulance.

In Chapter 2 the transducers used for control are characterised. This means that the electrical and mechanical properties were measured as they were used for modeling the mechanical system and designing the controller. In this chapter the design of a mechanical setup using ANSYS is presented. A simplification of the model is introduced which allows the system to be modeled as a lumped parameter model. Finally the models are compared with the measurements. In Chapter 3 the principle of electromagnetic shunt control is explained and implemented for two different types of controllers. In Chapter 4 it is explained how the synthetic impedance and the interfacing with dSpace was realised. In Chapter 5 the results of the controlled system are discussed for the two types of controllers used. The thesis is concluded in Chapter 6. The final results are discussed and recommendations for future work on the designed system are mentioned. Finally in the appendix, additional information can be found. It is explained in detail how the characterisation of the transducers was done. Also a quick reference manual for operating the system can be found.

2

Physical System Modeling

In this chapter the modeling of the physical mechanical system is presented. First, the characterisation of the electromagnetic transducer is presented in Section 2.1. Section 2.2 presents the distributed parameter model of the system and Section 2.3 the lumped parameter model. At the end of this chapter, a conclusion is given.

2.1 Transducer Model

The electromagnetic transducer used in this project is a 'Response CS2277 Power Bass Rocker', normally used for vibrating car seats while playing music as to enhance the experience of the low frequency range. Because a detailed datasheet elaborating on the important parameters of the transducer was not available, the transducer was characterised manually.

Figure 2.1 shows a cross section of the transducer. This transducer is quite

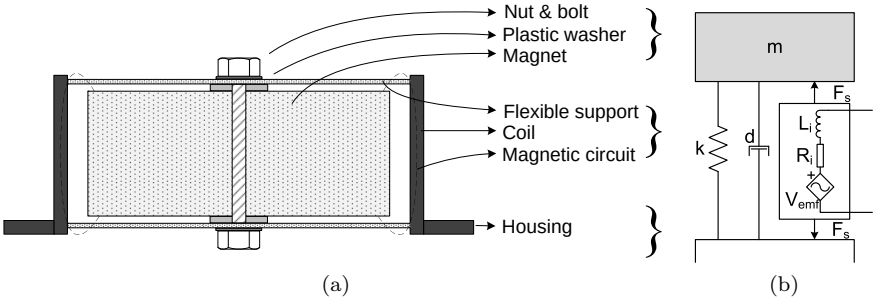

Figure 2.1: Transducer cross section (a) and model (b).

similar in structure to a normal loudspeaker. It consists of a coil which produces a magnetic field when a current is fed through. This will move the core magnet which is mounted inside the coil and supported by a flexible structure. The model used for this transducer is shown in Figure 2.1b. It is basically a mass-spring-damper system with an electrical port consisting of a coil, a series resistance and a voltage source modeling the back-emf voltage. The transducers

were assumed mechanically identical. Table 2.1 shows the measured mechanical parameters of the transducers.

Table 2.1: Mechanical parameters of the transducers.

Parameter	**Symbol**	**Value**
Spring constant	k	19037 N/m
Core mass	m	0.323 kg
Damping ratio	ζ	$3.39 \cdot 10^{-2}$
Damping Coefficient	d	5.32 Ns/m
Damped resonance frequency	ω_d	38.63 Hz
Resonance frequency	ω_c	38.65 Hz

The frequency range at which actuation is possible was found to be 20 Hz to 200 Hz for all transducers. However, they were not found to be electrically identical. Table 2.2 shows the measured electrical parameters of the transducers used for control (refer to Section 2.2.1).

Table 2.2: Electrical parameters of the three control transducers (T 1, 2 and 3).

Parameter	**Symbol**	**T 1**	**T 2**	**T 3**
Impedance at 50 Hz	Z_i [Ω]	3.6170	3.7204	3.8442
Inductance at 50 Hz	L_i [μH]	518	533	597
Resistance at 50 Hz	R_i [Ω]	3.6133	3.7166	3.8396
Current-Force coupling at 26.9 Hz	C_{iF} [N/A]	2.0523	3.6361	3.6996
Velocity-Voltage coupling at 26.9 Hz	C_{vV} [Vs/m]	2.0523	3.6361	3.6996

For a detailed description of the measurement procedures, refer to Appendix A.

2.2 Distributed Parameter Model

The goal of the project is to cancel one mode of vibration in the top plate of the system caused by vibrations coming in to the base plate. Because of this a simple setup of a system with only one mode of vibration which could be assumed a one-dimensional movement would suffice. However, as this was already done by Behrens [4] a more realistic setup mimicing the possible applications mentioned in Section 1.1 was desired. This setup then supports multiple modes of vibration, which can be studied in future work.

2.2.1 ANSYS system design

ANSYS Workbench was used to design a virtual setup, which is shown in Figure 2.2.

This system consists of four mechanically identical transducers mentioned in Section 2.1. The transducer indicated with '4' is used for inducing a vibration in the large MDF base plate which is supported by four rubber feet. Wood was used because it is cheap and not too heavy. The other three transducers are used as control transducers to cancel the vibration in the aluminium (6061-T6) top plate of 50x50 cm. Aluminium was chosen because it has a low damping

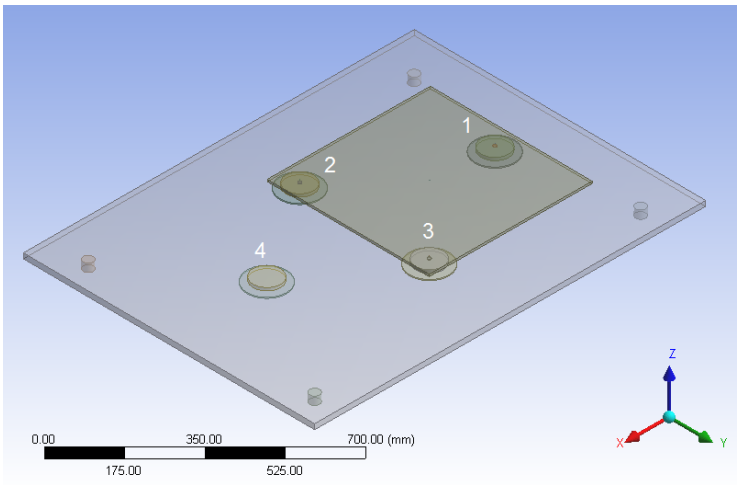

(a) Isometric view of the system model.

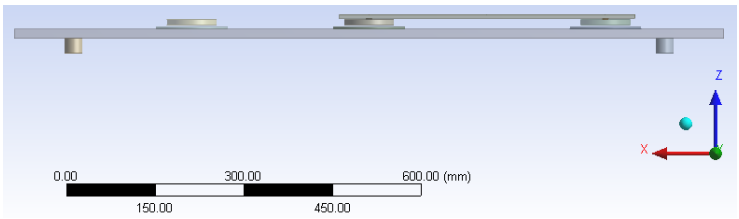

(b) Side view of the system model.

Figure 2.2: System model shown in isometric view (a) and side view (b). Note the three transducers used for controlling the top plate and one used for exciting vibrations in the base plate.

which is desired when vibrations need to be supported. The single transducer indicated with a '1' in Figure 2.2a is defined to be control transducer 1 and control transducer 2 and 3 are numbered counter-clockwise. Three transducers were used for controlling the top plate to ensure that the degrees of freedom of the top plate are not overconstrained. The position of the rubber feet and transducers was chosen such that the system showed multiple modes of vibration close to the resonance frequency of the transducers and well within the available transducer bandwidth of 20 Hz to 200 Hz.

2.2.2 System simulation

To verify that the system shows suitable behaviour, a harmonic response simulation was done. This simulation finds the modes of vibration of a chosen location as a result of a harmonic disturbance over a certain frequency range. The harmonic disturbance was placed at the disturbance transducer with a force amplitude of 10 N. Also, gravity on the entire model was present. Figure 2.3 shows the modes of vibration in the centre of the top plate.

It can be seen that the first mode of vibration is at 14 Hz which is below the frequency band of the transducer and therefore not suitable for control. The

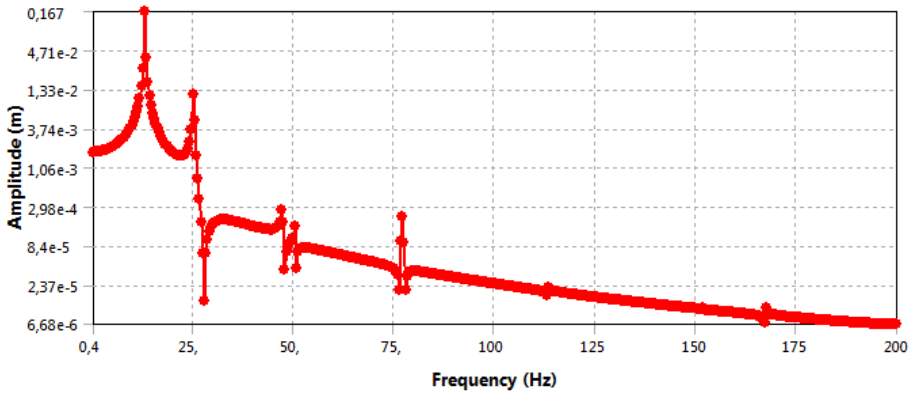

Figure 2.3: Response of the top plate to a harmonic disturbance at the disturbance transducer.

second mode at 25 Hz was chosen as the vibrational mode to cancel. Besides this, sufficient modes are present within the transducer bandwidth to allow for future research in multimode cancellation.

2.2.3 Model verification

The actual mechanical setup was built according to the setup made in ANSYS, which is shown in Figure 2.4.

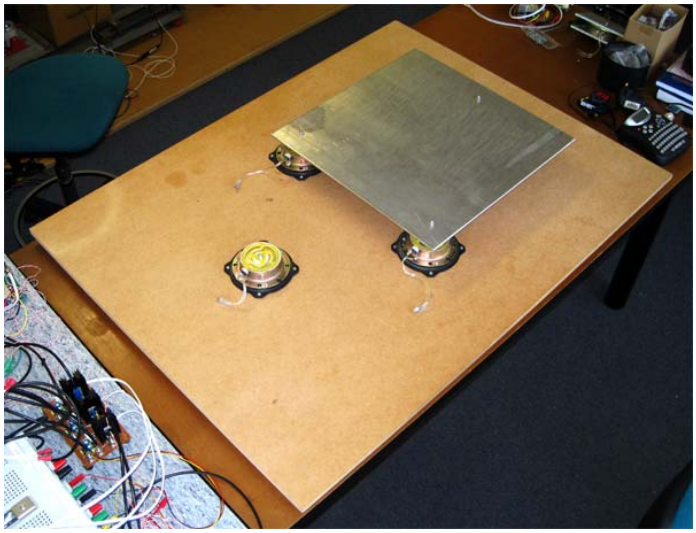

Figure 2.4: Completed setup of the mechanical system.

Harmonic response simulations were done at each transducer on the top plate in the same way as is described in Section 2.2.2. To verify this simulated behaviour to the actual setup, top plate measurements were done at the three control transducers.

Table 2.3: Simulated and measured resonance frequencies of the top plate at the three control transducers.

(a) Transducer 1

	Resonance frequency [Hz]
Simulated	14, 25, 50, 76, 113.
Measured	26.9, 36.8, 46.5, 78.4, 85.2, 121.6, 143.0, 196.4.

(b) Transducer 2

	Resonance frequency [Hz]
Simulated	14, 25, 48, 50, 76, 113, 168.
Measured	26.9, 36.8, 46.5, 76.3, 121.6, 142.5, 196.4.

(c) Transducer 3

	Resonance frequency [Hz]
Simulated	14, 25, 48, 50, 76, 113, 168.
Measured	26.9, 36.8, 46.5, 76.3, 78.0, 121.6, 142.5, 196.4.

The resonance frequencies at each transducer were determined by applying a harmonic disturbance to the base plate at the location of the disturbance transducer and measuring the acceleration at each control transducer with a PCB Piezotronics 353B17 accelerometer. Acceleration peaks indicate a resonance frequency at that particular disturbance frequency which was swept from 20 Hz to 200 Hz. Figure 2.6 shows the simulated harmonic response as well as the measured resonance frequencies, indicated by the vertical bars, at each transducer on the top plate. The resonance frequencies can also be found in Table 2.3.

It is observed that the measured resonance frequencies in the low frequency range up to 76.3 Hz approximate the simulated resonance frequencies quite well, except for the one at 36.8 Hz. In the high frequency range, only the measured peak at 121.6 Hz can approximate the simulated resonance frequency of 113 Hz, while the other two measured peaks are not found in simulations at all. This is probably due to unknown or neglected system dynamics.

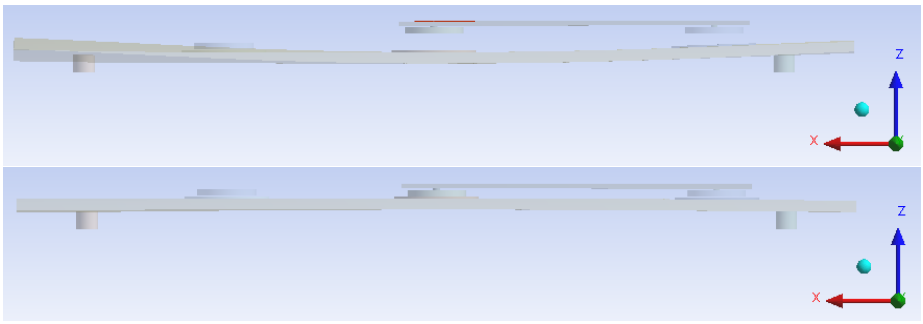

Figure 2.5: Out-of-phase movement of the top plate with respect to the base plate at 25 Hz.

At the simulated resonance frequency of 25 Hz the top plate shows an out-of-

phase movement with respect to the base plate, which is shown in Figure 2.5. This phase difference was measured at all control transducers at 26.9 Hz using two accelerometers as well. Besides vibrating along the z-axis, the top plate showed a tilting movement in the xz-plane as well. This is seen in the ANSYS model in Figure 2.5, where the two control transducers mounted in the middle of the base plate experience a larger deflection than the single transducer mounted to the right.

The model seemed to be in accordance with the real setup up to a frequency of 76.3 Hz and thus it was assumed competent for this low frequency range.

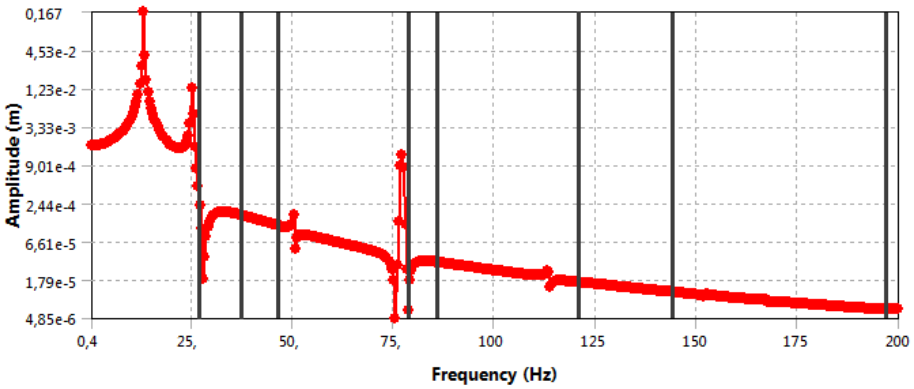

(a) Transducer 1

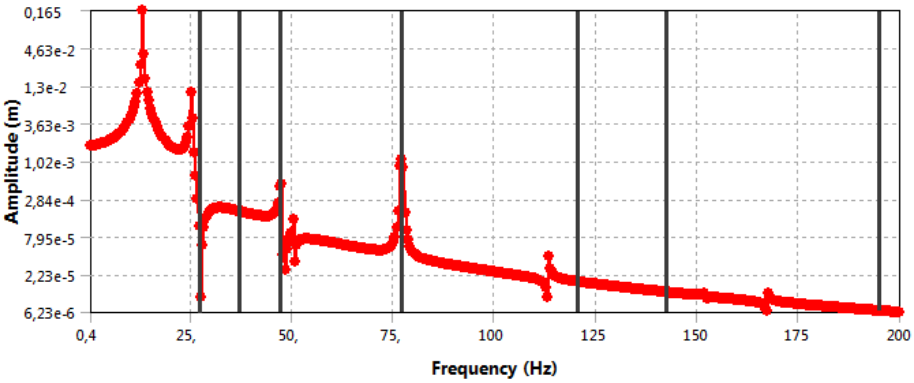

(b) Transducer 2

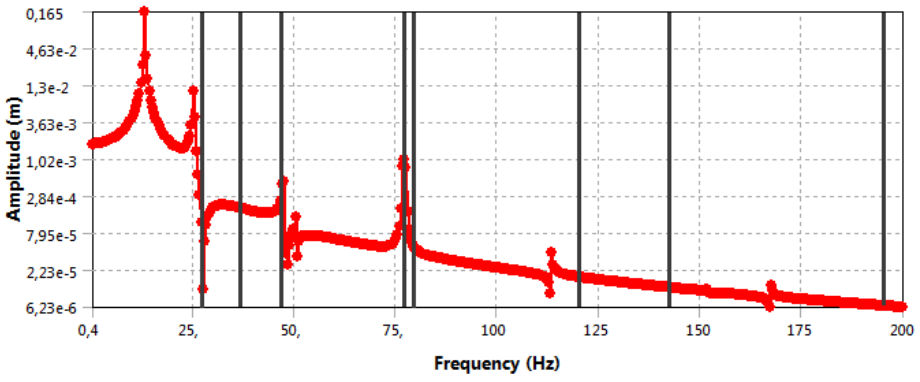

(c) Transducer 3

Figure 2.6: Simulated harmonic response and measured resonance peaks (vertical lines) of the top plate at transducer 1 (a), transducer 2 (b) and transducer 3 (c).

2.3 Lumped Parameter Model

From the ANSYS simulations it was observed that at the second vibration mode the plate is tilting and there exist no modes in the plate itself. Therefore, the system can be modeled as a lumped parameter model.

2.3.1 Spring-supported-beam

The system is modeled as a spring supported beam (see Figure 2.7). The plate is then depicted as the beam, where k_a and k_b are the stiffnesses of transducer 1 and transducer 2 and 3 combined respectively. Hence, the damping constants d_a and d_b represent the damping of transducer 1 and transducer 2 and 3 combined. Mass m represents the combined mass of the plate and the isolated masses of the transducer cores. Lengths a and b are the distances from transducer 1 and transducer 2 and 3 to the centre of rotation O. This centre of rotation was found to be at 0.09 m from A: this means that $a = 0.09$ m and $b = 0.31$ m.

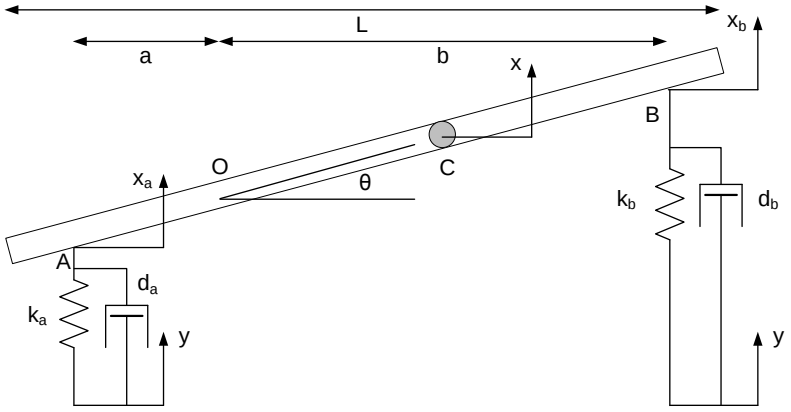

Figure 2.7: Spring-supported-beam model of the system.

The equations of motion can be derived for this system with the following equations:

$$\sum F_y = m\ddot{x}$$

$$\sum M_c = I_c\ddot{\theta}$$

If only small rotations are considered ($\sin\theta \approx \theta$), working out these equations gives the equations of motion:

$$\begin{bmatrix} m & 0 \\ 0 & I_c \end{bmatrix}\begin{bmatrix} \ddot{x} \\ \ddot{\theta} \end{bmatrix} + \begin{bmatrix} d_a + d_b & -d_a a + d_b b \\ -d_a a + d_b b & d_a a^2 + d_b b^2 \end{bmatrix}\begin{bmatrix} \dot{x} \\ \dot{\theta} \end{bmatrix} + \begin{bmatrix} k_a + k_b & -k_a a + k_b b \\ -k_a a + k_b b & k_a a^2 + k_b b^2 \end{bmatrix}\begin{bmatrix} x \\ \theta \end{bmatrix} = \begin{bmatrix} k_a + k_b & d_a + d_b \\ -k_a a + k_b b & -d_a a + d_b b \end{bmatrix}\begin{bmatrix} y \\ \dot{y} \end{bmatrix} \tag{2.1}$$

This system is described by x and θ. However, it is desired to write the system as a function of the displacement at the locations of the transducers: x_b and

x_a respectively. Here it is worked out for the transducers located at B. The equations of motion can be written in x_b and θ by using:

$$\begin{aligned} x_b &= x + b\theta \\ x &= x_b - b\theta \end{aligned} \tag{2.2}$$

By substituting Equation 2.2 into Equation 2.1, the equation of motion is written as a function of displacement x_b and angle θ:

$$\begin{aligned} &\begin{bmatrix} m & -mb \\ 0 & I_c \end{bmatrix} \begin{bmatrix} \ddot{x_b} \\ \ddot{\theta} \end{bmatrix} + \begin{bmatrix} d_a + d_b & -d_a a + d_a b \\ -d_a a + d_b b & d_a a^2 + d_a ab \end{bmatrix} \begin{bmatrix} \dot{x_b} \\ \dot{\theta} \end{bmatrix} + \\ &\qquad \begin{bmatrix} k_a + k_b & -k_a a + k_a b \\ -k_a a + k_b b & k_a a^2 + k_a ab \end{bmatrix} \begin{bmatrix} x_b \\ \theta \end{bmatrix} = \\ &\qquad\qquad \begin{bmatrix} k_a + k_b & d_a + d_b \\ -k_a a + k_b b & -d_a a + d_b b \end{bmatrix} \begin{bmatrix} y \\ \dot{y} \end{bmatrix} \end{aligned} \tag{2.3}$$

The system described by the equations above can be described in state space:

$$\dot{\mathbf{x}} = \mathbf{A}\mathbf{x} + \mathbf{B}\mathbf{u}$$

$$\mathbf{y} = \mathbf{C}\mathbf{x} + \mathbf{D}\mathbf{u}$$

Therefore the states of the system are defined to be:

$$\mathbf{x} = \begin{bmatrix} x_1 \\ x_2 \\ x_3 \\ x_4 \end{bmatrix} = \begin{bmatrix} x_b \\ \theta \\ \dot{x_b} \\ \dot{\theta} \end{bmatrix}$$

The system described by Equation 2.3 is written in the following form:

$$M\ddot{q} + C\dot{q} + Kq = B_0 y$$

Rewriting gives:

$$\ddot{q} = -M^{-1}C\dot{q} - M^{-1}Kq + M^{-1}B_0 y \tag{2.4}$$

Following the method described in Meirovitch [5], with Equation 2.3 and 2.4, the state space matrices are then defined as:

$$A = \begin{bmatrix} 0 & I \\ -M^{-1}K & -M^{-1}C \end{bmatrix}$$

$$B = \begin{bmatrix} 0 \\ M^{-1}B_0 \end{bmatrix}$$

C is a 4×1 matrix which defines the output of the system and can be chosen accordingly. Matrix D is zero in this case. The desired transfer function is from input velocity $sY(s)(= \varpi(s))$ to output velocity $sX_b(s)(= v_b(s))$:

$$G(s) = \frac{sX_b(s)}{sY(s)} = \frac{v_b(s)}{\varpi(s)} \left(= \frac{X_b(s)}{Y(s)} \right)$$

Using MATLAB, the desired transfer function can be derived from the state space system. For simulations, the values as listed in Table 2.4 were used.

Table 2.4: Parameter values used in MATLAB simulation.

Parameter	**Value**	**Unit**
m	5.39	kg
I_c	0.1462	$kg \cdot m^2$
k_a	19,037	N/m
k_b	38,074	N/m
d_a	5.32	Ns/m
d_b	10.64	Ns/m
L	0.50	m
Lab	0.40	m
a	0.09	m
b	0.31	m

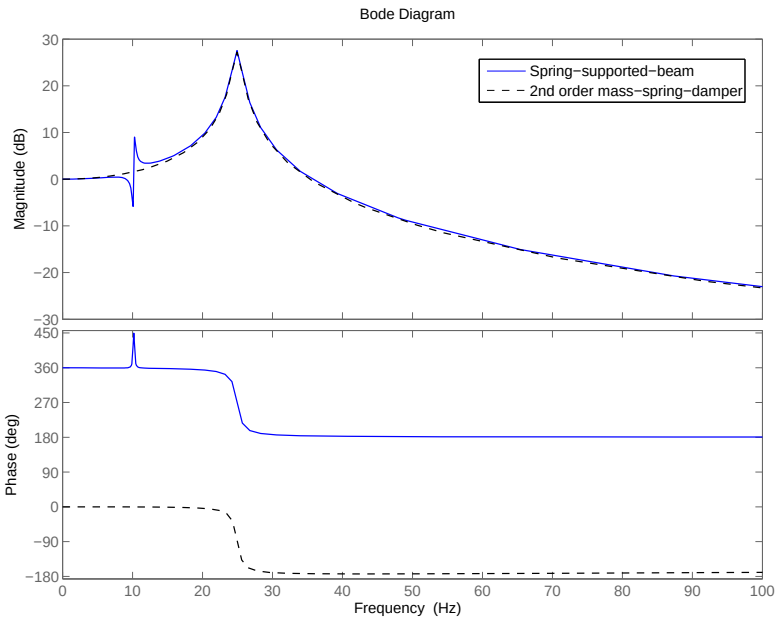

Figure 2.8: Transfer function $\frac{X_b(s)}{Y(s)}$ of the spring-supported-beam model compared to that of a mass-spring-damper model.

The spring-supported-beam model shows two modes of vibration: the first is at 10.3 Hz and the second mode is at 24.9 Hz. As stated in Section 2.2.2, the second mode is used for vibration isolation. Also shown in Figure 2.8 is the transfer of a mass-spring-damper system. As can be seen, the second mode of vibration can be accurately approximated by the mass-spring-damper model. This simplification into a second order model is useful when designing the controller.

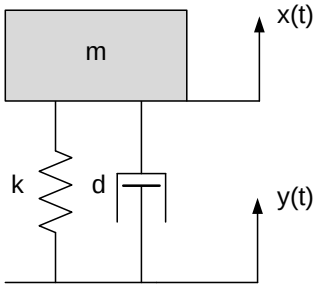

Figure 2.9: Model of mass-spring-damper system.

The equation of motion for the mass-spring-damper model is given by:

$$m\ddot{x}(t) + d\dot{x}(t) + kx(t) = d\dot{y}(t) + ky(t) \tag{2.5}$$

After applying the Laplace transform, the transfer from $Y(s)$ to $X(s)$ becomes

$$\frac{X(s)}{Y(s)} = \frac{ds + k}{ms^2 + ds + k} \tag{2.6}$$

By investigating the poles and zeros of the spring-supported-beam model, the mass m and stiffness k were calculated given a damping of 5.32 Ns/m. This resulted in a mass of 0.775 kg and a stiffness of 19037 N/m.

2.3.2 Model verification

It was proven that the spring-supported-beam model could be approximated by a mass-spring-damper model. In Figure 2.10 the transfer of the mass-spring-damper model is compared with the measured transfer. The base and top plate velocities were measured at the transducer mounting points. There is a significant difference in magnitude for the measured and simulated transfer. This is probably due to neglected effects in the model. However, the shape of the simulated transfer is almost the same. At transducers 2 and 3 the resonance peak is larger than at transducer 1. This is probably due to the system setup, transducers 2 and 3 are symmetrically placed with respect to the disturbance transducer and thus show similar behaviour.

The resonance frequency of the system is different from the resonance frequency derived with the spring-supported-beam model: a resonance at 24.6 Hz was measured instead at 24.9 Hz. Therefore the mass in the mass-spring-damper model was adjusted such that resonance occurred at 24.6 Hz. In Figure 2.11 the velocity of the top plate is shown. As can be seen, maximum velocity does not occur at the resonance frequency of the transfer between base and top plate. This is caused by the fact that the supporting base plate also has its own modes of vibration. In this case there is a mode at 26.9 Hz which causes the base to resonate and this vibration is coupled into the top plate. So coupling between base plate and top plate is maximum at 24.6 Hz but the maximum top plate velocity is at 26.9 Hz.

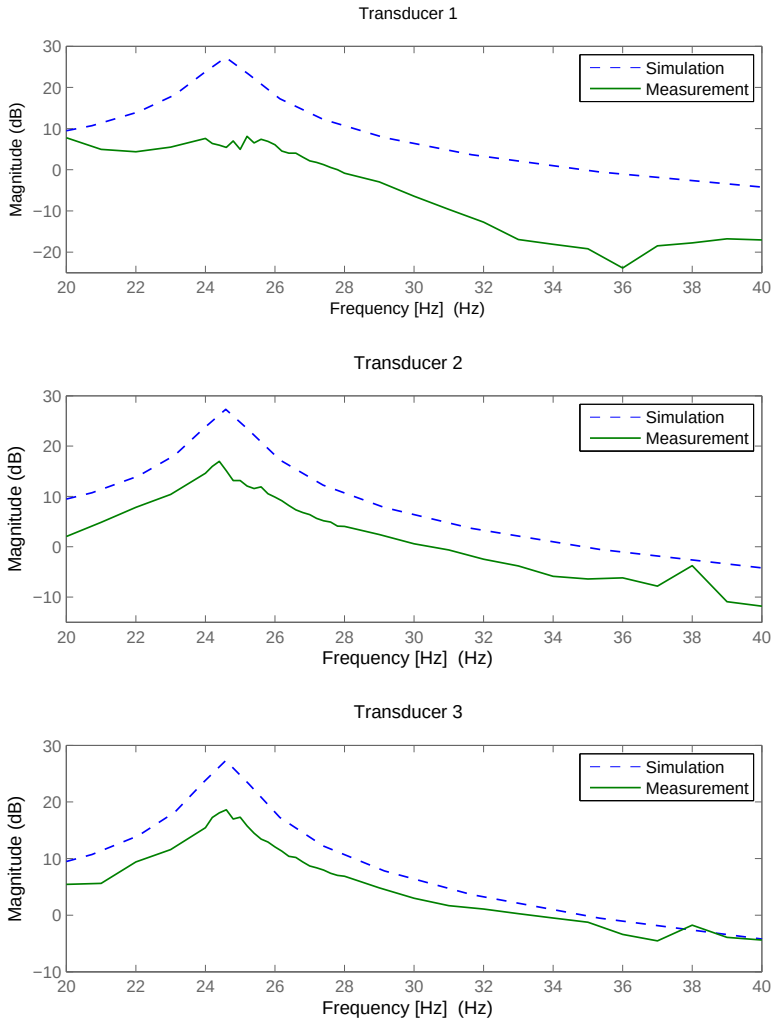

Figure 2.10: The simulated transfer compared to the measured transfer.

2.4 Conclusion

The mechanical system was designed in ANSYS and an actual setup was built according to this design. The model was verified using the setup and found to be competent up to a frequency of 76.3 Hz. A lumped parameter model was made for the vibrational mode at 24.6 Hz. This spring-supported-beam model was approximated by a second order mass-spring-damper system to simplify the controller design.

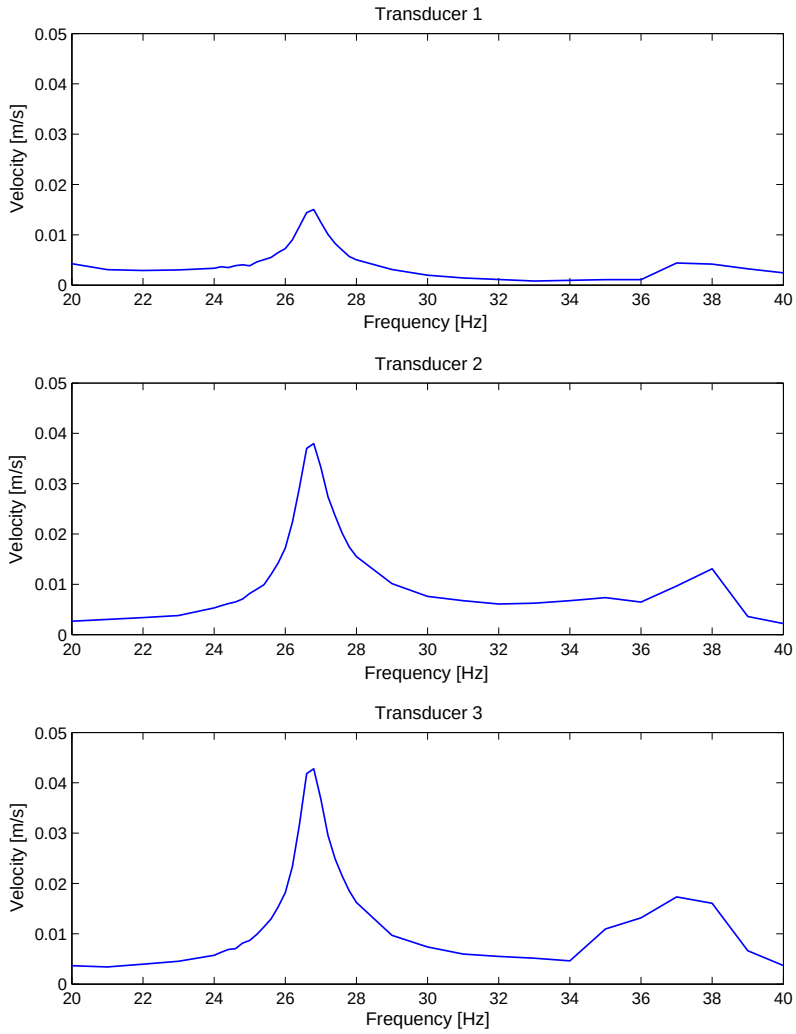

Figure 2.11: Top plate velocity at the three control transducers.

3

Controller Design

An electromagnetic shunt controller is used to realise vibration isolation. In this chapter it will be explained what electromagnetic shunt control means and what type of shunt controller was used. Three transducers are used to control vibration in the top plate. These transducers are controlled individually, this means that the system is regarded as having three inputs and three outputs. So it is considered to consist of three SISO systems. The input of each SISO system is the shunt current for the control transducer and the output is the force generated by the transducer.

3.1 Electromagnetic Shunt

In electromagnetic shunt control an electrical impedance is connected to the terminals of an electromagnetic tranducer with the aim to control vibration. When a relative velocity is put into the transducer, an electrical voltage is induced (back-emf) across the terminals of the transducer according to:

$$V_{emf}(t) = C_{vV} v_{in}(t) \tag{3.1}$$

When an impedance is connected to the terminals, a shunt current $I_s(t)$ is generated. This shunt current then will generate a force equal to:

$$F_s(t) = C_{iF} I_s(t) \tag{3.2}$$

The direction of this force is the opposite of the direction of the velocity input. This means that the force counteracts the vibration and hence the vibration will be reduced.

The electrical impedance is designed such that it will satisfy the vibration isolation problem as described in Chapter 1. In Figure 3.1 the electrical equivalent circuit of an electromagnetic transducer is shown. As can be seen, a shunt impedance $Z_s(s)$ is connected to the terminals of the transducer. The force generated by the transducer depends on the shunt current $I_s(s)$. The shunt current is defined as follows:

$$I_s(s) = \frac{V_s(s)}{Z_s(s)} \tag{3.3}$$

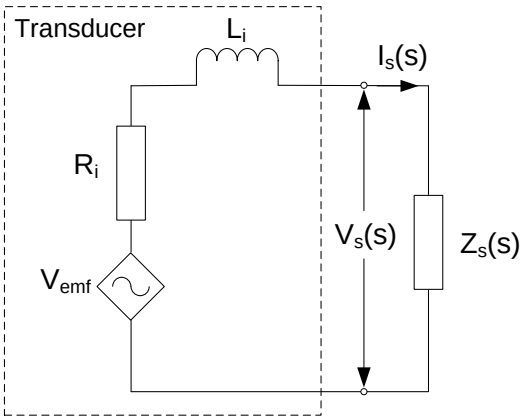

Figure 3.1: Electrical circuit of an electromagnetic transducer with a shunt impedance connected.

The voltage $V_s(s)$ depends on the generated back-emf and the impedance of the circuit:

$$V_s(s) = \frac{Z_s(s)}{R_i + sL_i + Z_s(s)} V_{emf}(s) \tag{3.4}$$

Using Equation 3.3 and 3.4, the shunt current is written as:

$$I_s(s) = \frac{1}{R_i + sL_i + Z_s(s)} V_{emf}(s) \tag{3.5}$$

Substituting Equation 3.1 and 3.2 in Equation 3.5 gives the expression for the generated shunt force as a function of the relative velocity input and the shunt impedance:

$$F_s(s) = \frac{C_{vV} C_{iF}}{R_i + sL_i + Z_s(s)} v_{in}(s) \tag{3.6}$$

For the shunted electromagnetic transducer it means that a shunt force F_s is added to the model of the mass-spring-damper in Section 2.3, as shown in Figure 3.2.
The equation of motion for the shunted transducer is:

$$m\ddot{x}(t) + d\dot{x}(t) + kx(t) + F_s(t) = d\dot{y}(t) + ky(t) \tag{3.7}$$

Applying the Laplace transform gives:

$$(ms^2 + ds + k)X(s) + F_s(s) = (ds + k)Y(s) \tag{3.8}$$

Substituting Equation 3.6 with $v_{in}(s) = sX(s) - sY(s)$ into Equation 3.8 gives:

$$(ms^2 + ds + k)X(s) + \frac{C_{vV} C_{iF}}{R_i + sL_i + Z_s(s)}(sX(s) - sY(s)) = (ds + k)Y(s) \tag{3.9}$$

For simplicity, it is assumed that:

$$K(s) = \frac{C_{vV} C_{iF}}{R_i + sL_i + Z_s(s)} \tag{3.10}$$

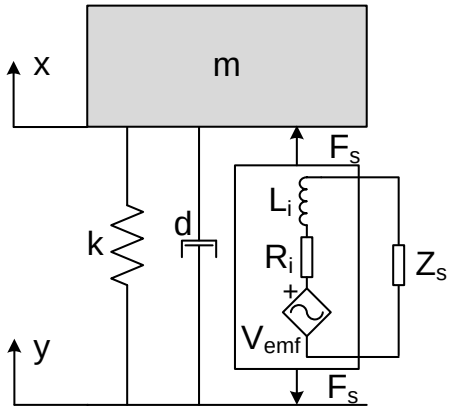

Figure 3.2: Shunted electromagnetic transducer.

Substituting $K(s)$ into Equation 3.9:

$$(ms^2 + (d + K(s))s + k)X(s) = ((d + K(s))s + k)Y(s) \tag{3.11}$$

This gives the transfer $G_{\varpi v}(s)$ from base plate velocity $\varpi(s)(= sY(s))$ to top plate velocity $v(s)(= sX(s))$ for the shunted electromagnetic transducer:

$$G_{\varpi v}(s) = \frac{X(s)}{Y(s)} = \frac{v(s)}{\varpi(s)} = \frac{(d + K(s))s + k}{ms^2 + (d + K(s))s + k} \tag{3.12}$$

Substituting Equation 3.10 into Equation 3.12 gives the transfer for the shunted electromagnetic transducer:

$$G_{\varpi v}(s) = \frac{(d + \frac{C_{vV}C_{iF}}{R_i + sL_i + Z_s(s)})s + k}{ms^2 + (d + \frac{C_{vV}C_{iF}}{R_i + sL_i + Z_s(s)})s + k} \tag{3.13}$$

3.2 RC-controller

Different types of electromagnetic shunt controllers exist. Their main difference lies in the way the impedance Z_s is implemented. One possibility is to implement the shunt impedance with a series resistor-capacitor (RC) circuit. It was proven by Behrens [4] that the RC-controller is very effective around the resonance frequency, but has limited attenuation at higher frequencies. Because of its effectiveness at resonance and its simplicity, the RC-controller was chosen for shunt control.

The RC-controller is based on an RLC-resonator which consists of the combined resistance of the transducer and shunt circuit ($R_t = R_i + R_s$), the inductance of the transducer (L_i) and the capacitance of the shunt circuit (C_s). The resonator should have its resonance peak at the vibration mode of interest. The resonance frequency is determined by the inductance and capacitance:

$$\omega_c^2 = \frac{1}{L_i C_s} \tag{3.14}$$

This means that the capacitance can be calculated once the resonance frequency is known:

$$C_s = \frac{1}{L_i \omega_c^2} \tag{3.15}$$

It was shown that the resonance frequency of the mass-spring-damper system is determined by the mass and stiffness:

$$\omega_c^2 = \frac{k}{m} \tag{3.16}$$

Now the shunt capacitance can be expressed in m and k:

$$C_s = \frac{1}{L_i \frac{k}{m}} = \frac{m}{L_i k} \tag{3.17}$$

The shunt impedance Z_s is now defined as:

$$Z_s(s) = R_s + \frac{1}{sC_s} = \frac{sR_sC_s + 1}{sC_s} \tag{3.18}$$

Using Equation 3.13 and 3.18 gives the closed-loop transfer for the RC shunted system:

$$G_{\varpi v}(s) = \frac{(d + \frac{C_{vV}C_{iF}}{R_i + sL_i + \frac{sR_sC_s+1}{sC_s}})s + k}{ms^2 + (d + \frac{C_{vV}C_{iF}}{R_i + sL_i + \frac{sR_sC_s+1}{sC_s}})s + k} \tag{3.19}$$

As was explained in Section 1.1, an increase in system damping results in peak resonance reduction but decreases the high-frequency roll-off. This means that a trade-off between peak resonance reduction and high-frequency attenuation has to be made. The total resistance R_t determines the amount of damping for the shunted system. The transducer resistance R_i is fixed. Therefore, R_s has to be chosen such that peak resonance is achieved but at the same time the high frequency attenuation is still acceptable. An optimisation principle will be used to find the optimal value for the shunt resistance.

It was shown by Behrens [4] that by minimising the H_2 norm of the closed-loop system $G_{\varpi v}(s)$, the optimal value for the shunt resistance can be determined. This is due to the fact that the H_2 norm of the system is related to the area under its magnitude response. The H_2 norm of the closed-loop system is defined as [2]:

$$\|G_{\varpi v}(s)\|_2 = \left(\int_{-\infty}^{\infty} trace(G_{\varpi v}(s)^* G_{\varpi v}(s)) ds \right)^{\frac{1}{2}}$$

Referring to the vibration isolation principle, the goal was to have peak resonance reduction and high-frequency attenuation. This means that the area under the transfer function has to be minimised. The H_2 norm is related to this area. By calculating the H_2 norm for a range of values for the shunt resistance, the optimal value for the shunt resistance R_s can then be determined by investigating for which shunt resistance the H_2 norm is minimal:

$$R_{s,opt} = argmin \, \|G_{\varpi v}(s)\|_2$$

3.2.1 Implementation RC-controller

The second mode of vibration is the mode of interest, this was found to be at 24.6 Hz. But as was shown, maximal top plate velocity occurs at 26.9 Hz. Because the main goal is reducing vibrations in the top plate, the frequency of 26.9 Hz is used in the design of the controller. However, the transfer between base plate and top plate will be used to calculate the optimal shunt resistance. Therefore the mass-spring-damper model is still used, but the shunt circuit is designed such that maximum damping is at 26.9 Hz. For the resonant frequency of 24.6 Hz it can be calculated what the corresponding mass is using:

$$m = \frac{k}{(2\pi f_n)^2}$$

For a spring constant of 19037 N/m, the mass is 0.797 kg. The shunt capacitances are now calculated with Equation 3.15 using the frequency of 26.9 Hz. The three control transducers were found to have different inductances. This results in different shunt capacitances for each transducer as is shown in Table 3.1.

MATLAB was used to calculate the H_2 norm of the closed loop transfer (see Equation 3.19) for a range of shunt resistor values. This was done for each control transducer as there are small differences in their electrical parameters. The optimal values found for R_s are listed in Table 3.1. In Figure 3.3 it is shown how the H_2 norm changes as a function of the shunt resistance for transducer 3.

Table 3.1: Electrical parameters for each of the three control transducers for the RC-shunt.

Parameter	**Symbol**	**T 1**	**T 2**	**T 3**
Resistance	R_i	3.6133 Ω	3.7166 Ω	3.8396 Ω
Inductance	L_i	$518 \cdot 10^{-6}$ H	$533 \cdot 10^{-6}$ H	$597 \cdot 10^{-6}$ H
Coupling	C_{vV}, C_{iF}	2.0523	3.6361	3.6996
Shunt capacitance	C_s	$67.58 \cdot 10^{-3}$ F	$65.68 \cdot 10^{-3}$ F	$58.64 \cdot 10^{-3}$ F
Shunt resistance	R_s	−3.5492 Ω	−3.5690 Ω	−3.6842 Ω

3.2.2 RC-controller simulation

In Figure 3.4 the transfer of the open-loop system is compared to the closed-loop system. The RC-controller introduces significant peak response reduction. However, as expected the high-frequency attenuation has decreased because of the increase in system damping.

The transfer for the shunt circuit is defined as:

$$\frac{I_s(s)}{V_{emf}(s)} = \frac{1}{Z_i(s) + Z_s(s)} \tag{3.20}$$

For the RC shunt circuit, with $Z_s(s) = \frac{sR_sC_s+1}{sC_s}$, this means that the transfer will become:

$$\frac{I_s(s)}{V_{emf}(s)} = \frac{1}{R_i + sL_i + \frac{sR_sC_s+1}{sC_s}} = \frac{sC_s}{s^2L_iC_s + s(R_i+R_s)C_s + 1} \tag{3.21}$$

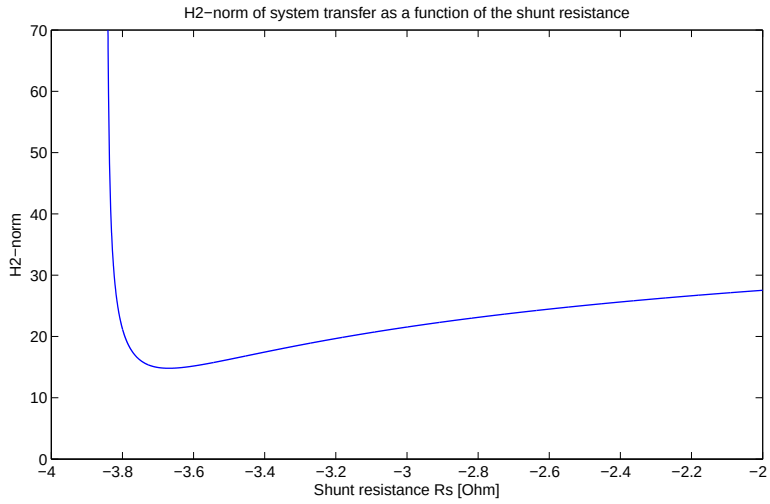

Figure 3.3: H_2 norm of the system transfer as a function of the shunt resistance (transducer 3).

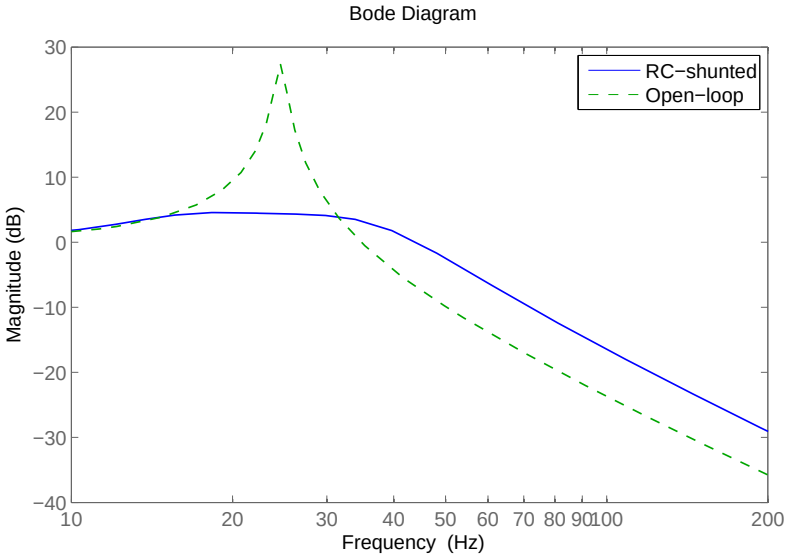

Figure 3.4: The open-loop system transfer compared to the RC shunted transfer.

A bode plot of this transfer is shown in Figure 3.5. The parameters for the third transducer were used in the transfer. The transfer has a maximum amplitude at 26.9 Hz, which means that most force will be generated by the transducer at the resonance frequency of the system since $F_s(s) = C_{iF} I_s(s)$.

From the bode plot it can be seen that the bandwidth of the RC-controller is large compared to the system bandwidth. The bandwidth (in Hz) of a series

RLC circuit is given by:

$$BW = \frac{R}{2\pi L} \tag{3.22}$$

This means that the system with the RC-controller has a bandwidth of 45 Hz. This is large compared to the bandwidth of the system which is 20 Hz to 200 Hz. The realised mechanical system has vibration modes at higher frequencies. Using the RC-controller it is not possible to target these modes individually because of this high bandwidth. In Section 3.3 a different type of resonant shunt controller is proposed which solves this problem.

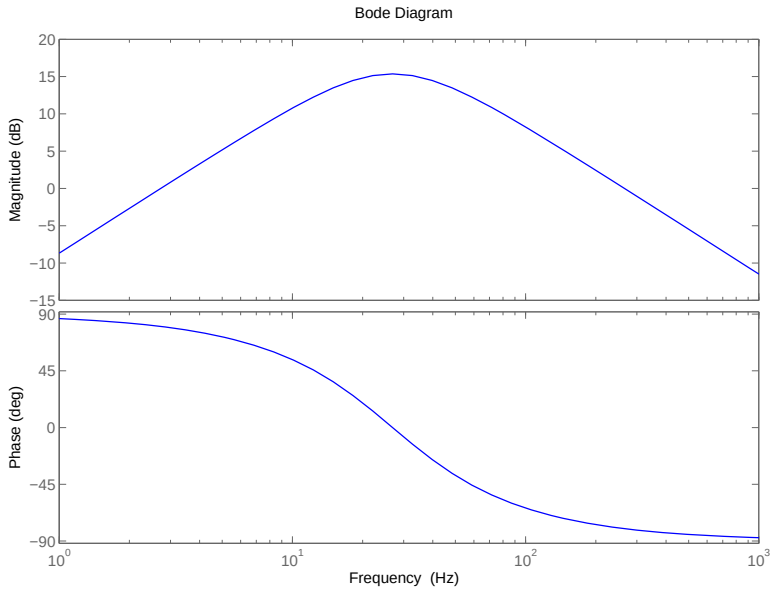

Figure 3.5: Transfer of RC shunt circuit combined with the transducer electronics: $\frac{I_s(s)}{V_{emf}(s)}$.

3.3 RLC-controller

In this paragraph a different type of resonant controller is introduced: the RLC-controller. The RLC-controller is almost similar to the RC-controller, the only difference is that an inductance is added to the shunt circuit. It was shown that the bandwidth of an RLC circuit is determined by the resistance and the inductance (Equation 3.22). By adding an inductance to the shunt circuit, the total inductance can be increased and hence the bandwidth will decrease. This allows designing a controller which can target a single mode of vibration, as opposed to the previous RC-controller. Although this is not of importance for vibration isolation, it may prove valuable when one is interested in controlling multiple modes for the system.

By adding an inductance L_s to the shunt circuit, the shunt impedance becomes:

$$Z_s(s) = R_s + sL_s + \frac{1}{sC_s} = \frac{s^2 L_s C_s + sR_s C_s + 1}{sC_s} \tag{3.23}$$

This means that the transfer of the RLC-controller is given by:

$$\frac{I_s(s)}{V_{emf}(s)} = \frac{1}{Z_i(s) + Z_s(s)} = \frac{sC_s}{s^2(L_i + L_s)C_s + s(R_i + R_s)C_s + 1} \tag{3.24}$$

3.3.1 Implementation RLC-controller

The RLC-controller has to be designed such that it will control the mode of interest, and will leave other modes unaffected. The bandwidth of this controller is then chosen accordingly to the bandwidth of the mode of interest.

Once the bandwidth and total resistance are known, the total inductance is calculated by:

$$L_{tot} = \frac{R_{tot}}{2\pi BW} \tag{3.25}$$

The shunt capacitance is calculated by:

$$C_s = \frac{1}{(\omega_n)^2 L_{tot}} \tag{3.26}$$

The bandwidth for the mode at 26.9 Hz was found to be 1.5 Hz. From the simulations with the RC-controller it was found that a total resistance of 0.1 Ω would give good peak resonance damping. The H_2 norm optimisation approach can not be used here since that would change the total resistance of the circuit and hence the bandwidth of the controller will also be changed. The inductance and capacitance values for the three control transducers were calculated and are also listed in Table 3.2.

Table 3.2: Electrical parameters for the RLC-controller.

Parameter	**Symbol**	**T 1**	**T 2**	**T 3**
Resistance	R_i	3.6133 Ω	3.7166 Ω	3.8396 Ω
Inductance	L_i	$518 \cdot 10^{-6}$ H	$533 \cdot 10^{-6}$ H	$597 \cdot 10^{-6}$ H
Coupling	C_{vV}, C_{iF}	2.0523	3.6361	3.6996
Shunt resistance	R_s	−3.5133 Ω	−3.6166 Ω	−3.7396 Ω
Shunt inductance	L_s	$10.09 \cdot (10^{-3})$ H	$10.08 \cdot (10^{-3})$ H	$10.01 \cdot (10^{-3})$ H
Shunt capacitance	C_s	$3299 \cdot 10^{-6}$ F	$3299 \cdot 10^{-3}$ F	$3299 \cdot 10^{-3}$ F

3.3.2 RLC-controller simulation

Using the values for transducer 3 from Table 3.2, the RLC-shunted system was simulated (Figure 3.6). Compared to the RC-controller, the RLC controller shows good performance at the resonance frequency. Because of the narrow bandwidth of the RLC-controller, the shunted system shows two peaks above and below the resonance frequency of the system.

In Figure 3.7 the response of the RLC-controller is shown. As expected, it shows a narrow resonance peak and will have little effect on frequencies other than the resonance frequency.

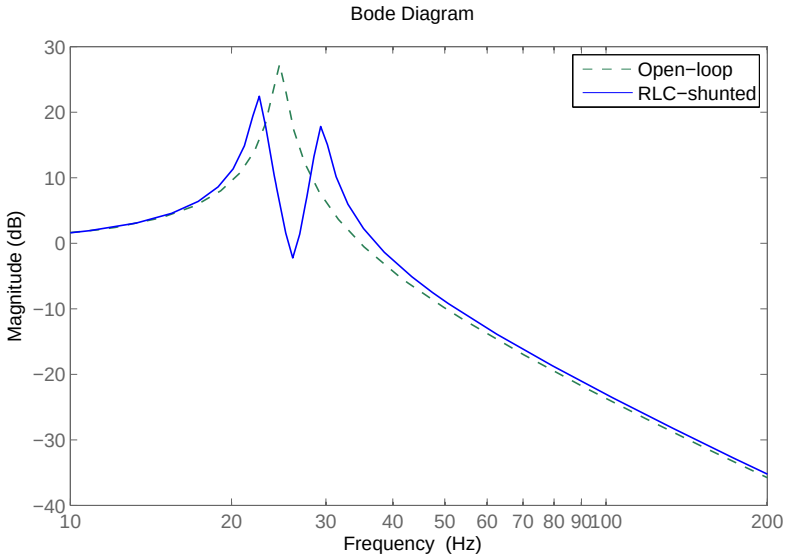

Figure 3.6: Open-loop transfer compared to the RLC shunted transfer.

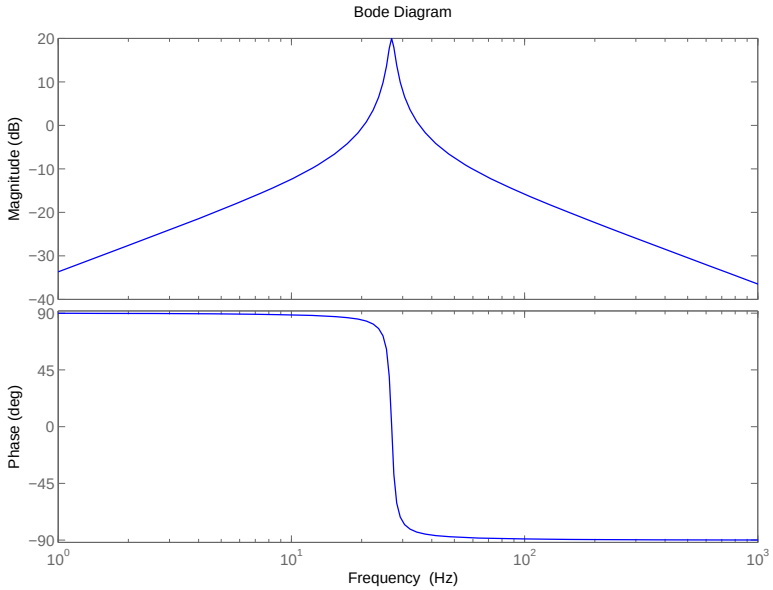

Figure 3.7: Transfer of RLC shunt circuit combined with the transducer electronics: $\frac{I_s(s)}{V_{emf}(s)}$.

3.4 Conclusion

Two different type of controllers were designed and implemented. From the simulations it was expected that the RC-controller would give good results concerning the vibration isolation problem, which means peak resonance reduction and attenuation at high frequencies. The RLC-controller on the other hand has a narrow resonance peak which will make it useful in controlling multiple modes.

4

System Design & Realisation

In this chapter the design and realisation of the system will be presented. Figure 4.1 shows a complete model for the shunt control as implemented in MATLAB Simulink. Three paths can be recognised, as there are three control transducers each using two inputs and one output. The blocks 'Shunt control' and 'Self sensing' are described in Section 4.1 and Section 4.2 respectively. The interfacing ports are described in Section 4.3.

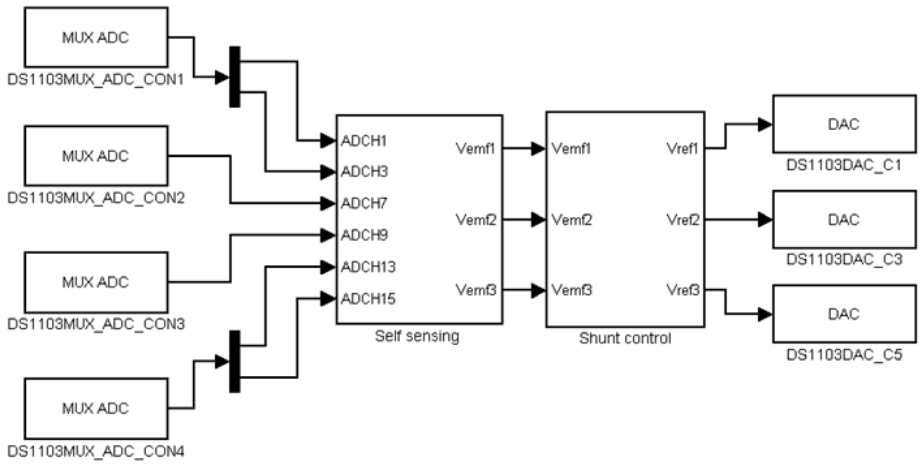

Figure 4.1: Complete shunt control model as implemented in MATLAB Simulink.

4.1 Synthetic Shunt Impedance

Typically shunt circuits are implemented using a network of physical components. This has some important disadvantages:

- The network is tuned to a specific resonance frequency, so if a system parameter changes which causes a shift in the resonance frequency, the network is useless. Therefore, a passive network is not suitable for adaptive vibration control.
- For multiple mode damping, the circuit size can become quite large as a seperate shunt circuit has to be realised for each mode of vibration.
- Depending on the mechanical system and type of transducer, the component values can get quite large, e.g. up to thousands of Henries, according to Behrens [3], when using a piezo transducer.

To overcome these disadvantages a synthetic impedance is used to implement the shunt circuit.

A synthetic shunt impedance is basically an impedance synthesized in a digital signal processor (DSP) which can provide an arbitrary relationship between the voltage and current at its terminals, seen in Figure 4.2.

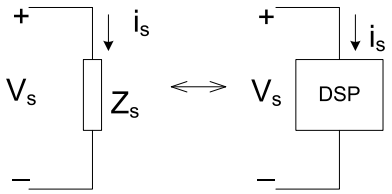

Figure 4.2: Shunt impedance Z_s and synthetic shunt impedance as programmed in a DSP.

By fixing the current $I_s(s)$ to be the output of a linear transfer function of the voltage $V_s(s)$ (a voltage controlled current source or VCCS), any network of physical components $Y_s(s)$ can be synthesized:

$$I_s(s) = Y_s(s) \cdot V_s(s). \tag{4.1}$$

As the shunt impedance is connected to the terminals of the transducer, a series network of the internal transducer impedance and shunt impedance is formed as seen in Figure 3.1. The transfer from the back-emf voltage $V_{emf}(s)$ to the shunt current $I_s(s)$ is given in Equation 3.5. This model was implemented in MATLAB Simulink using a block diagram which is shown in Figure 4.3. Three of these block diagrams were placed in the 'Shunt control' block in Figure 4.1), as there are three control transducers.
Via Mason's rule the transfer function of this block diagram from $V_{emf}(s)$ to $I_s(s)$ is given by:

$$I_s(s) = \frac{\frac{1}{L_i s + R_i}}{1 + \frac{1}{L_i s + R_i} \cdot Z_s} \cdot V_{emf} = \frac{1}{L_i s + R_i + Z_s} \cdot V_{emf} \tag{4.2}$$

which is indeed equal to Equation 3.5. The shunt current $I_s(s)$ is then multiplied by the shunt impedance Z_s to get a reference shunt voltage as the output instead of a reference current. This reference voltage is placed across the shunt

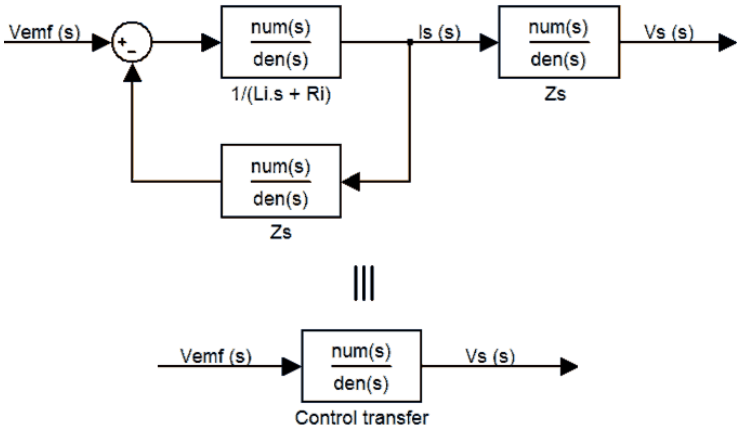

Figure 4.3: MATLAB Simulink model of the synthetic impedance.

impedance and thus across the transducer, as this voltage would be the response of the physical shunt impedance to the current $I_s(s)$ as a result of the induced back-emf voltage $V_{emf}(s)$. The circuitry to achieve this is presented in Section 4.3.

The following transfer functions were implemented in the 'Control transfer' block of the MATLAB Simulink model seen in Figure 4.3. In case of the RC-shunt controller:

$$\frac{V_s(s)}{V_{emf}(s)} = \frac{Z_s}{Z_i + Z_s} = \frac{sR_sC_s + 1}{s^2L_iC_s + s(R_i + R_s)C_s + 1} \tag{4.3}$$

and in case of the RLC-shunt controller:

$$\frac{V_s(s)}{V_{emf}(s)} = \frac{Z_s}{Z_i + Z_s} = \frac{s^2L_sC_s + sR_sC_s + 1}{s^2(L_i + L_s)C_s + s(R_i + R_s)C_s + 1} \tag{4.4}$$

4.2 Self Sensing

The synthetic impedance outputs a current which depends on the back-emf voltage V_{emf}, according to Equation 4.2. To be able to calculate the current through the shunt impedance and thus the reference voltage that needs to be put across the transducer, the back-emf voltage needs to be known. The main problem here is that both the reference voltage output and the back-emf voltage generated by the transducer appear at its terminals. Therefore, these two voltages need to be seperated before the back-emf voltage can be measured.

4.2.1 Operating principle

To measure the back-emf voltage without using any additional sensors, a technique called 'self-sensing' was used [6]. The transducer is then used for actuation and sensing at the same time, which means that actuation and sensing are performed collocated. Figure 4.4 shows an electrical model of an electromagnetic transducer in series with a measurement resistor R_m.

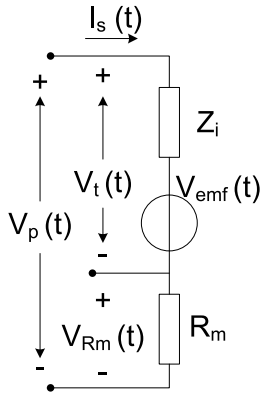

Figure 4.4: Principle of the self-sensing technique used to measure the back-emf voltage V_{emf}.

From this figure, it can be seen that:

$$V_t(t) = V_{Zi} + V_{emf}. \tag{4.5}$$

V_{emf} is now easily found:

$$V_{emf}(t) = V_t(t) - V_{Zi} = V_t(t) - Z_i \cdot I_s(t) = V_t(t) - Z_i \cdot \frac{V_{Rm}(t)}{R_m}. \tag{4.6}$$

This is shown in a block diagram in Figure 4.5. The $V_{emf}(t)$ at the output is then fed to the block diagram seen in Figure 4.3. When implemented in MATLAB Simulink this time domain block diagram is converted to the frequency domain.

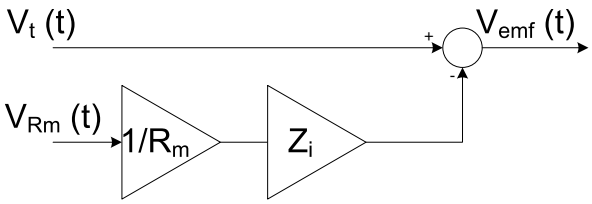

Figure 4.5: Block diagram for the calculation of the back-emf voltage.

The internal transducer impedance Z_i is known as this was characterised (Chapter 2.1) and because R_m is known, the back-emf voltage can be calculated by measuring the voltage across the transducer $V_t(t)$ and across the measurement resistor $V_{Rm}(t)$. A 1 Ω measurement resistor with a power rating of 5 W was chosen to be used in series with the transducer such that the current flowing through the transducer would not be limited severely and thereby also limiting the input voltage $V_p(t)$ (Figure 4.4) necessary for applying a certain voltage $V_t(t)$ across the transducer. Three of these block diagrams are placed in the 'Self sensing' block in Figure 4.1 to accomodate for the three control transducers.

4.2.2 Verification measurements

The performance of the self-sensing measurement technique was measured using all three control transducers and evaluated with the accelerometer measurements. The transducers were connected in series with a 0.9859 Ω resistor (with a power rating of 5 W) and powered using a sinusoidal signal at 26.9 Hz. The current $I_s(t)$ was calculated by measuring the voltage across the resistor and dividing it by the resistance. Using the voltage across the transducer and the specific coupling coefficients and impedances, the velocity of the core was calculated by means of the back-emf generated by the shaker. This velocity was verified with the velocity calculated by measuring the acceleration of the top plate and base plate using accelerometers (PCB Piezotronics 353B17) in the same way as described in Section A.5. Table 4.1 lists the measured values.

Table 4.1: Transducer core velocity measurement by the self sensing method and verification by accelerometers at 26.9 Hz.

(a) Transducer 1

	$\mathbf{V_{back\text{-}emf}}$ **[m/s]**	$\mathbf{V_{accelerometers}}$ **[m/s]**	**Difference [%]**
Measurement 1	0.0025	0.0007	73.09
Measurement 2	0.0028	0.0054	90.53
Measurement 3	0.0034	0.0081	141.77
Average			101.80

(b) Transducer 2

	$\mathbf{V_{back\text{-}emf}}$ **[m/s]**	$\mathbf{V_{accelerometers}}$ **[m/s]**	**Difference [%]**
Measurement 1	0.0957	0.0840	12.25
Measurement 2	0.1134	0.1057	6.83
Measurement 3	0.1270	0.1170	7.92
Average			9.00

(c) Transducer 3

	$\mathbf{V_{back\text{-}emf}}$ **[m/s]**	$\mathbf{V_{accelerometers}}$ **[m/s]**	**Difference [%]**
Measurement 1	0.0952	0.0838	11.97
Measurement 2	0.1111	0.0963	13.28
Measurement 3	0.1262	0.1099	12.90
Average			12.72

It can be seen that the velocity measurements using the self sensing method is comparable to the velocity measured using the accelerometers in case of transducer 2 and 3, as the average absolute difference between the two methods is around 10 %. However, the velocity measurement in case of transducer 1 is not. This is due to the fact that the velocity at transducer 1 is much smaller than at the other transducers and is therefore more sensitive to errors in the parameters used for calculating the velocity via the self sensing method. When the measurement resistance value is varied between its lower and upper bound regarding the measurement error of the RCL-meter (Equation A.18), the absolute difference varies between 0 % and more than 200 %, while this does not cause a significant change in the absolute difference in the measurements of transducers 2 and 3.

4.3 Electronics

4.3.1 dSpace

To be able to acquire the back-emf voltage and to output the reference transducer voltage a dSpace DS1103 Controller Board was used to interface with the system. This board provides 16 16-bit analog-to-digital (AD) converters, 4 12-bit AD converters and 8 14-bit digital-to-analog (DA) converters. When running a simulation externally in MATLAB Simulink, the onboard DSP is used for the signal processing and acquisition and output of the various signals via its AD and DA converters. The continuous model in Simulink is then discretised and run at a sampling rate of 10 kHz, which was found to be sufficient by looking at the representation of a 26.9 Hz sinusoidal signal. A samping rate of 1 kHz would show a staircase approximation of the same sinusoid, which is undesired.

For a list of the AD and DA converters used, refer to Table 4.2. Only the 16-bit AD converters were used instead of the 12-bit, to minimise the quantisation error.

Table 4.2: AD and DA converters on the dSpace DS1103 used for signal acquisition and reference voltage output.

Signal	**Symbol**	**T 1**	**T 2**	**T 3**
Reference voltage	V_{in}	DACH1	DACH3	DACH5
Transducer voltage	V_t	ADCH1	ADCH7	ADCH13
Measurement resistor voltage	V_{Rm}	ADCH3	ADCH9	ADCH15

4.3.2 Interfacing circuits

The MATLAB Simulink model needs the transducer and measurement resistor voltages to calculate the back-emf and a control signal. Subsequently, the output voltage needs to be put across the transducer. Figure 4.6 shows a block diagram of one of the interface circuits used to power the control transducers as well as to measure the transducer and measurement resistor voltage. Because there are three control transducers, this circuit was built in triplicate.

In this figure, U_1 represents the OPA548 power operational amplifier and U_2 and U_3 represent the generic uA741 operational amplifier configured as a differential amplifier with a gain of 1. R_m indicates a measurement resistor used for calculating the current flowing through the transducer and is specific for each circuit, because the self sensing measurement depends on an accurate value of this resistance. Table 4.3 lists the different resistor values.

Table 4.3: Specific measurement resistor value for each interface circuit.

Circuit	**Symbol**	**Value [Ω]**
1	R_{m1}	1.0000
2	R_{m2}	0.9859
3	R_{m3}	0.9935

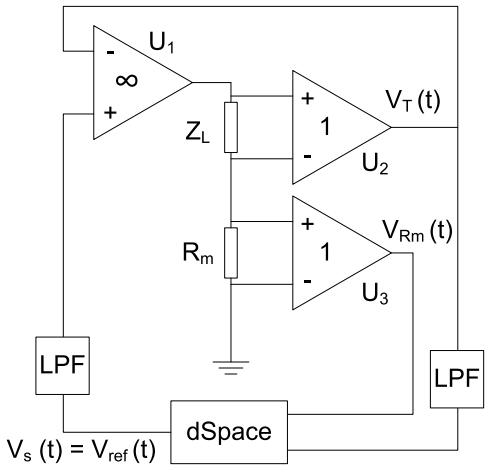

Figure 4.6: The interface circuit used to power the control transducer and to measure its voltage and the measurement resistor voltage for the purpose of self sensing.

The transducer voltage $V_t(t)$ measured across the transducer which is represented by Z_L and measurement resistor voltage $V_{Rm}(t)$ are acquired by the dSpace AD converters and after calculating the back-emf voltage V_{emf}, the control signal is output by the dSpace DA converter. This is the reference voltage which is placed across the transducer, using the negative feedback loop via U_2. Simple first order low-pass filters (LPF) with a cut-off frequency of 1591 Hz (using a 1 kΩ resistor and 100 nF capacitor) were placed at the input of the transducer voltage measurement and after the dSpace output to reduce high frequency noise. The V_{Rm} input was not filtered as this was not necessary and even deteriorated the signal.

For a detailed circuit schematic, refer to Appendix B.

4.3.3 Additional electronics

To induce vibrations in the system, the disturbance transducer was powered by a 50 W JayCar amplifier kit. A sinusoid was used as input signal, which was swept from 20 to 40 Hz.

4.4 Conclusion

In this chapter, the design of the system was presented. The designed shunt controller is implemented as a synthetic impedance using MATLAB Simulink and dSpace. For calculating the control action, the back-emf voltage of the transducers is needed, which is measured using a self sensing method. This means that the same transducer is used for measuring and actuation. Electronic circuits to be used as an interface between the system and dSpace were designed which can offer the proper measurements as well as handle the reference voltage to be put across the transducer, i.e. the control signal.

5

Results & Measurements

In this chapter the results and perfomance of the RC-controller and RLC-controller will be compared and discussed. Measurements were done with a single transducer shunted and three transducers shunted at the same time. The differences between these measurements are also compared and discussed.

5.1 Measurement Setup

For the measurements the system was disturbed by the disturbance transducer, an input signal of 250 mV peak to peak was used for the JayCar audio amplifiers. The frequency was swept from 20 Hz to 40 Hz for all measurements. Accelerometers were used to determine the velocity of the base plate and top plate. The base and top plate velocities were measured at the mounting points of the transducers.

The measurements were interpreted in two ways: first a transfer is derived from the measurements which is compared to the theory. Secondly the top plate velocity is shown, this velocity is used to discuss the performance of the control strategies as the main interest lies in reducing the top plate velocity. Measurements were done for the following configurations:

- System with transducer 3 RC-shunted
- System with all three transducers RC-shunted
- System with transducer 3 RLC-shunted
- System with all three transducers RLC-shunted

As was explained in Chapter 3, the system is considered to consist of three SISO systems. This is questioned since it is expected that there will be coupling between the inputs and outputs of each SISO system. By comparing measurements for a single shunted transducer and three shunted transducers it is investigated what the effect is of having three transducers shunted. It is expected that performance will worsen because the three transducers work independently from one another. This means that control effects from one transducer can have a negative effect on the output of another transducer.

5.2 Results RC-controller

Measurements were done with the RC-controller with the parameters as calculated in Table 3.1. However, the optimal shunt resistance could not be used when all three control transducers were shunted at the same time. The RC-controller has a large overshoot at a step input which results in a large current for a short time when control is turned on. This is not a problem when a single transducer is shunted, but when three are shunted at the same time, not enough current was supplied by the power supply. This problem was solved by increasing the damping of the RC-circuit, i.e. by increasing the total resistance of the shunt circuit. For a total resistance of 0.4 Ω it was found that the overshoot was decreased enough for the power supply to supply the required current.

5.2.1 Single control transducer

In Figure 5.1 the transfer between base plate and top plate is shown when transducer 3 is shunted. The optimal determined shunt resistance was used and the shunt circuit was designed to have maximum damping at 26.9 Hz (see values in Table 3.1). The shunt circuit gives a peak resonance reduction as was expected. Referring to Chapter 1, an increase in damping will cause lower high-frequency attenuation. This is supported by the measument: at higher frequencies the shunted system has lower attenuation than the open-loop system.

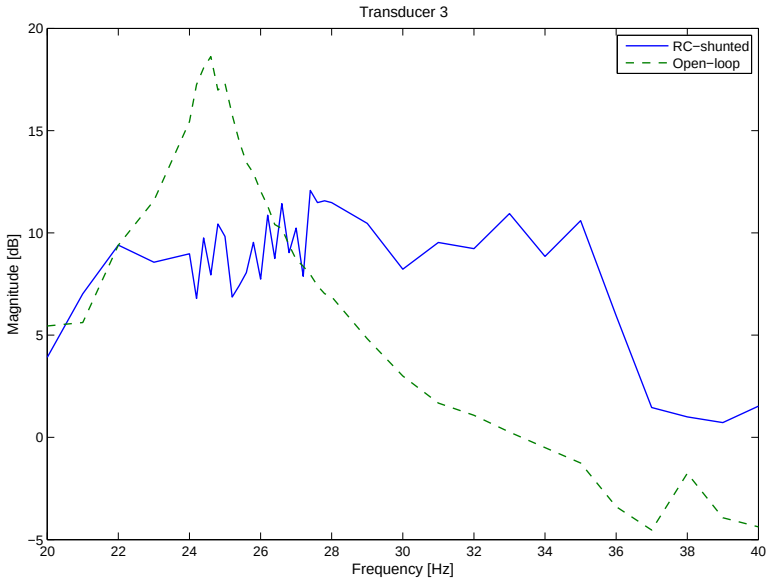

Figure 5.1: Transfer between base and top plate with transducer 3 RC-shunted measured at transducer 3.

In Figure 5.2 is is shown that the RC-shunt reduces the vibrations in the top plate. A reduction of 11.8 dB was achieved at 26.9 Hz.

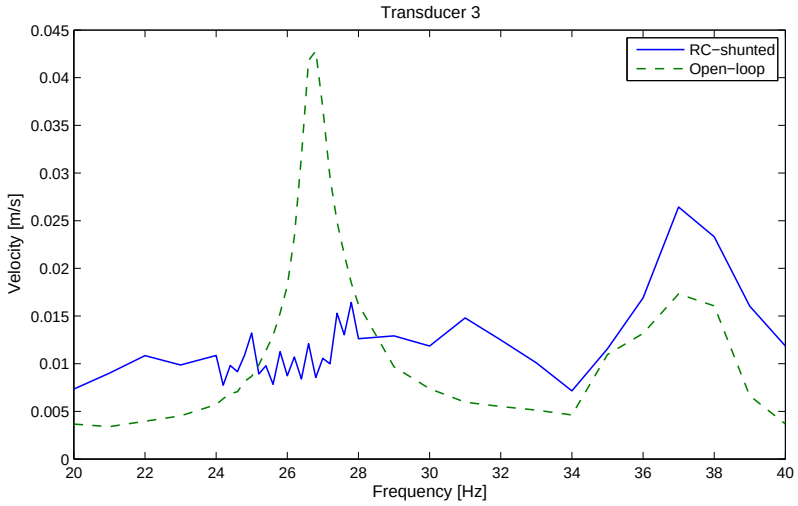

Figure 5.2: Top plate velocity when transducer 3 is RC-shunted measured at transducer 3.

5.2.2 Three control transducers

In Figure 5.3 the transfer for all three transducers is shown when they are all shunted. At transducer 2 and 3 the transfer shows peak resonance reduction, but at transducer 1 no reduction in peak resonance can be seen. It is shown that the high-frequency attenuation has decreased again with respect to the open-loop transfer.

In Figure 5.4 the top plate velocities are shown at the three transducers when they are all shunted. For all transducers the top plate velocity has decreased at the resonance frequency (see Table 5.1). However, reduction of top plate velocity at resonance has decreased compared with the situation when only transducer 3 was shunted. Thus it seems that when all transducers are controlled, performance decreases.

It can be seen that for low frequencies the top plate velocity has increased. This effect could already be seen for the single shunted transducer, but for three shunted transducers this effect has even worsened. This effect is probably caused by noise in the circuits which are used to power the control transducers. Even when the disturbance transducer is turned off little vibrations could be measured when control was turned on.

Table 5.1: Reduction in top plate velocity at the three control transducers when all transducers are shunted.

Transducer	**Open-loop [m/s]**	**RC-shunt [m/s]**	**Reduction [dB]**
1	0.01504	0.00665	7.1
2	0.03797	0.01898	6.0
3	0.04279	0.01644	8.3
3 (T 3 shunted)	0.04279	0.01095	11.8

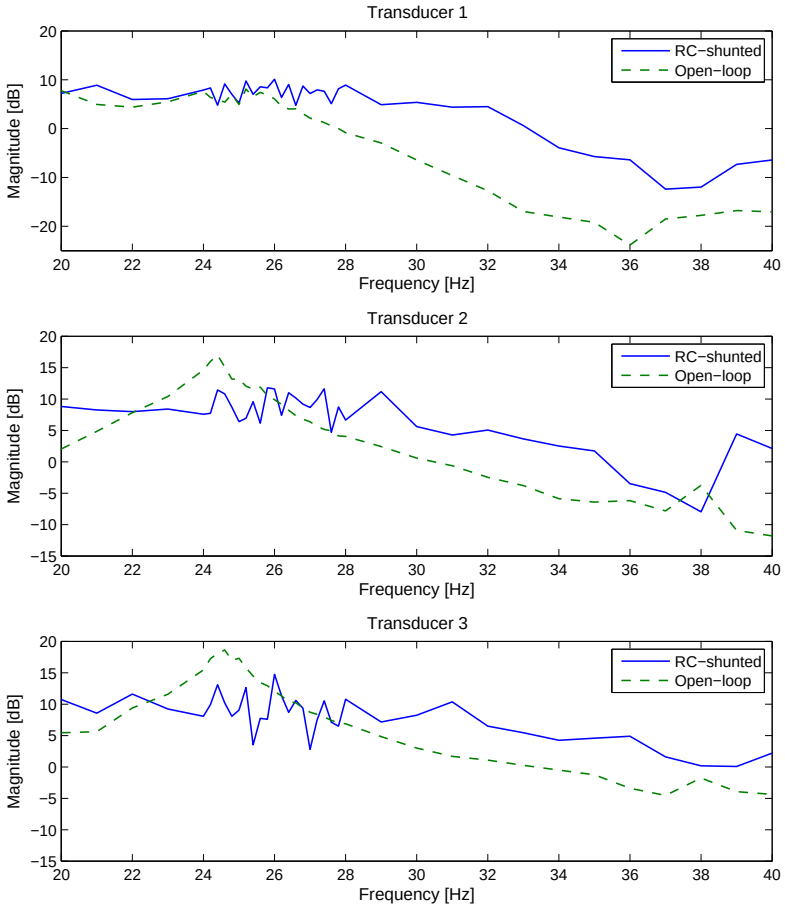

Figure 5.3: Transfer between base and top plate when all transducers are RC-shunted, measured at the transducers.

The control effect of a shunted transducer will depend on the location on the top plate. For the situation of the single shunted transducer and for three shunted transducers, the top plate velocity was measured at transducer 3. By measuring the top plate velocity in the centre of the top plate, it was investigated whether performance will also decrease at a different location when all transducers are controlled.

In Figure 5.5 the results of the measurement in the centre of the plate are shown. As expected, in both situations peak resonance has reduced. However, in the centre of the plate there is no significant difference in peak resonance reduction with a single shunted transducer or three shunted transducers. For the single shunted transducer a peak reduction of 11.5 dB was measured compared with a peak reduction of 12.1 dB for three shunted transducers.

More measurements would be needed to be able to tell something about

the effect of treating the total system as three SISO systems. It seems that it depends where the measurement is performed whether a change in performance is measured. Therefore, in future work a MIMO approach should be used to be able to draw any conclusions about the performance of the system as three SISO systems.

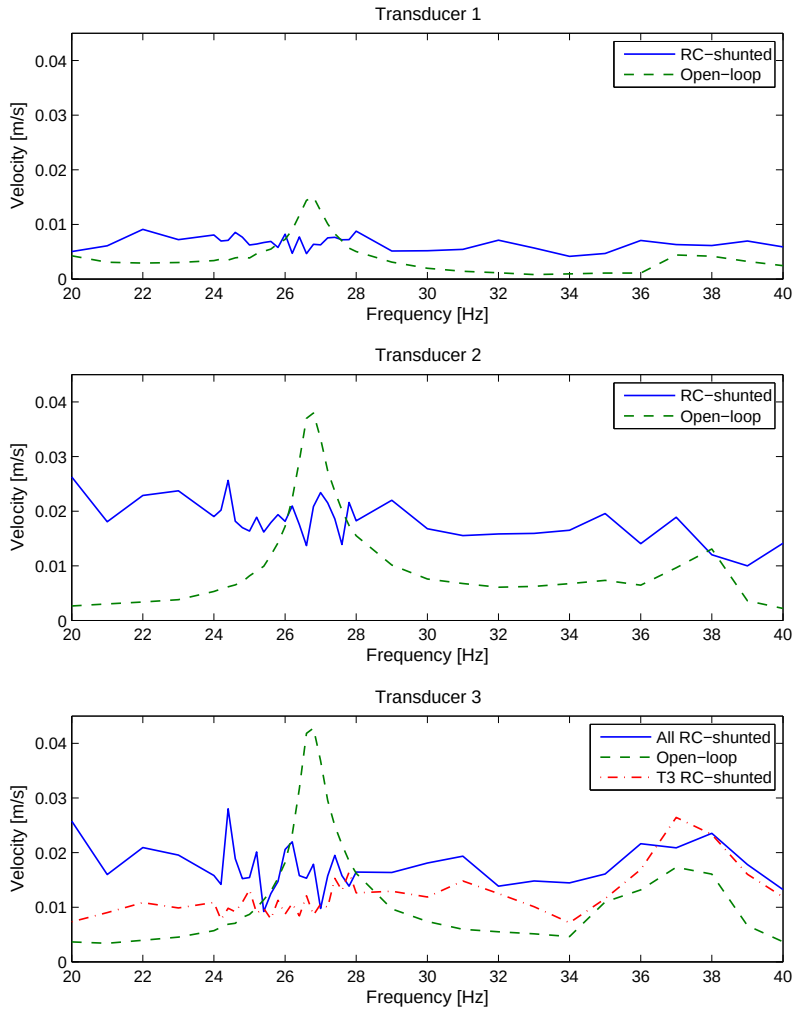

Figure 5.4: Top plate plate velocities when all transducers are RC-shunted, measured at the transducers.

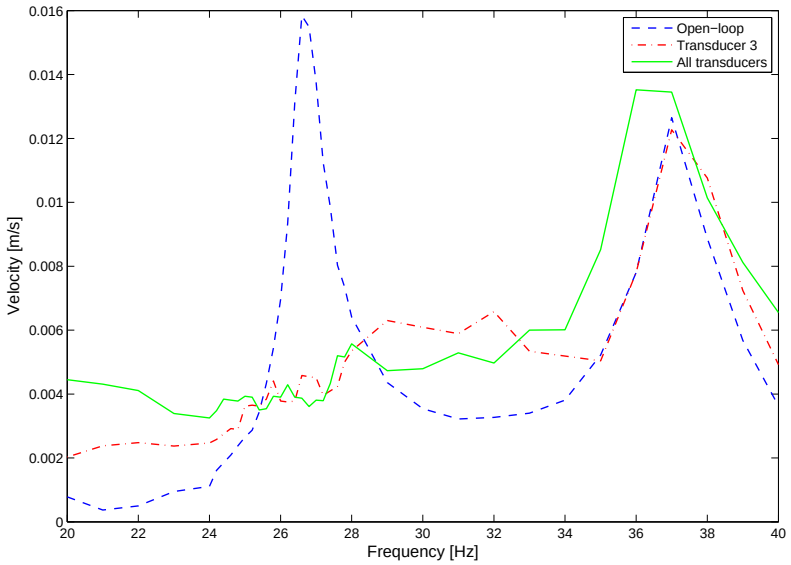

Figure 5.5: Velocity in the centre of the plate measured with: open-loop, transducer 3 RC-shunted and three transducers RC-shunted.

5.3 Results RLC-controller

Measurements were done with the RLC-controller with the parameters as calculated in Table 3.2. For the single shunted transducer a total resistance of 0.1 Ω was taken. The problem with large currents also occurred here when all transducers were shunted at the same time. By changing the total resistance to 0.8 Ω this problem was overcome. However, changing the resistance results in a larger bandwidth of 12 Hz instead of 1.5 Hz. This is kept in mind when discussing the measurements.

5.3.1 Single control transducer

In Figure 5.6 the transfer between base and top plate is shown when control transducer 3 was shunted. As expected, the transfer has peak resonance reduction which is maximal at 26.9 Hz at which the system was designed to have maximum damping effect. Because the RLC-controller has a small bandwidth, the transfer shows high gains above and below 26.9 Hz. The transfer shows high gains at higher frequencies, this is not supported by the theoretical response in Figure 3.6 where the shunted transfer only has little reduction in high frequencies. A possible explanation for the difference could be the phase shift which is introduced by the controller. When this phase shift is large, the generated shunt force will be in phase with the disturbance velocity and the vibration will be amplified. This was not researched and therefore it is not known what the precise cause is for the high gain at the higher frequencies.

In Figure 5.7 the top plate velocity at transducer 3 is shown. The RLC-shunt results in a large reduction in top plate velocity at 26.9 Hz. A reduction in top plate velocity of 16.4 dB was measured. The plate velocity is increased at frequencies other than the resonance frequency. It should be noted that bandwidth was increased to 12 Hz by changing the total resistance, so this could be an explanation for the difference in transfer at high frequencies. The precise cause for this is not known and should be researched in future work.

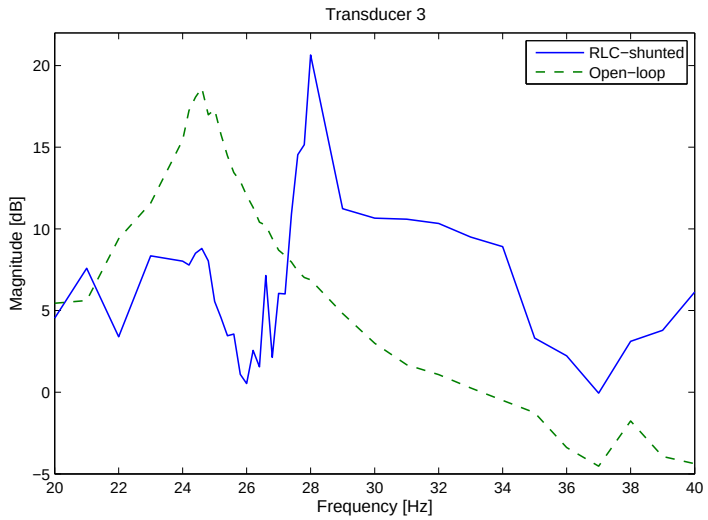

Figure 5.6: Transfer between base and top plate with transducer 3 RLC-shunted.

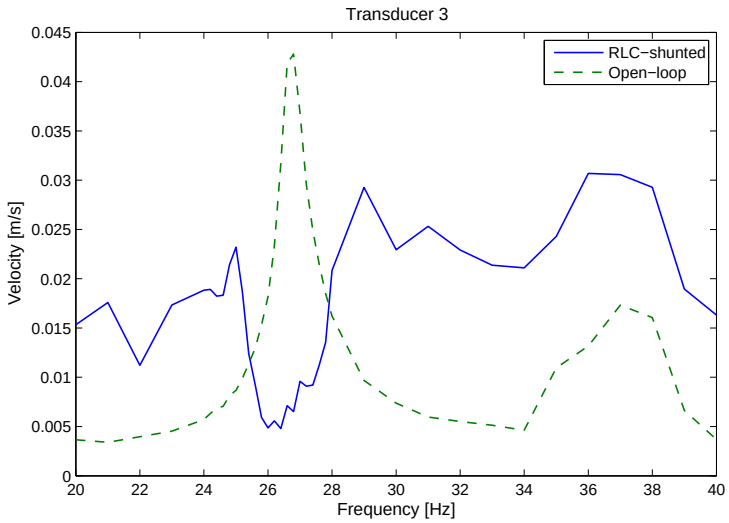

Figure 5.7: Top plate velocity when transducer 3 is RLC-shunted.

5.3.2 Three control transducers

In Figure 5.8 the transfers at the three transducers are shown when all transducers are RLC-shunted. In all transfers, a reduction in gain is shown at 26.9 Hz, the frequency at which the system was designed to have maximum damping. Also an increase in transfer is seen above and below 26.9 Hz which is in agreement with the theoretical response. In contrast to the single shunted system, the transfer at transducer 3 does not show an increase at high frequencies.

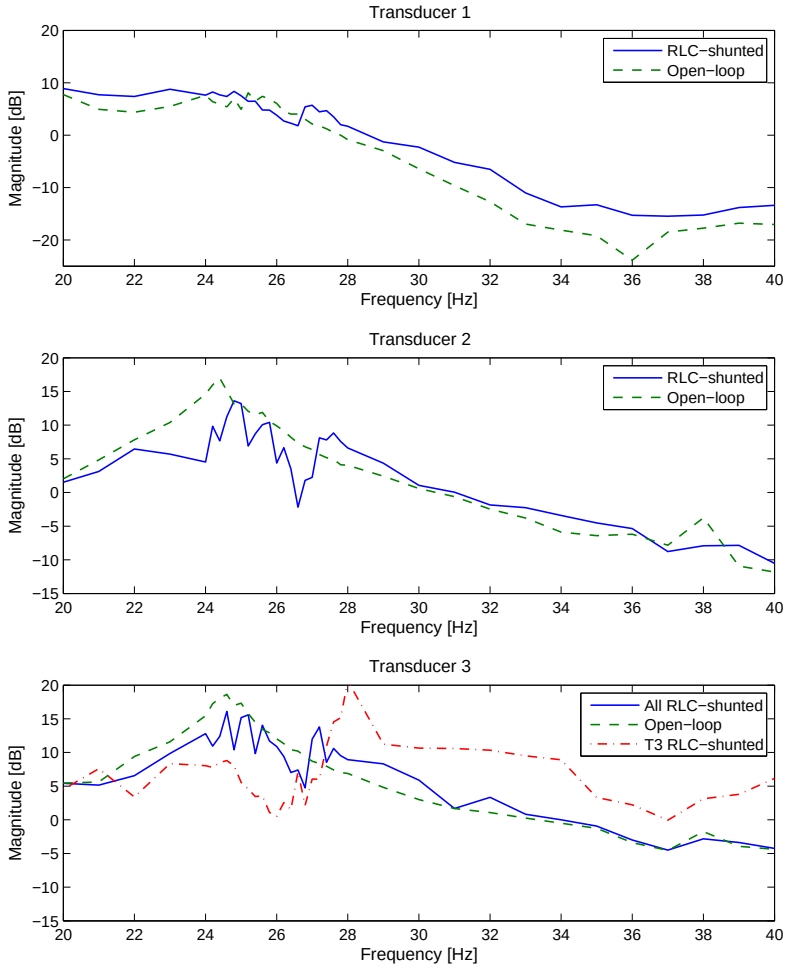

Figure 5.8: Transfer between base and top plate when all transducers are RLC-shunted, measured at the transducers.

In Figure 5.9 the top plate velocities are shown at the different transducers when all transducers are RLC-shunted. All transducers show a significant reduction in top plate velocity at 26.9 Hz (see Table 5.2). With the RLC shunt, there is

no difference in resonance peak reduction at transducer 3 for the single shunted system and three transducer shunted system. So it seems that there is less coupling effect between the transducers. However, this should be investigated in future work as this was not confirmed in this thesis. In contrast to the single shunted system, the top plate velocity does not change for each transducer at higher and lower frequencies when all transducers are shunted.

Table 5.2: Reduction in top plate velocity at the three control transducers when all transducers are shunted.

Transducer	**Open-loop [m/s]**	**RLC-shunt [m/s]**	**Reduction [dB]**
1	0.01504	0.00384	11.9
2	0.03797	0.00586	16.2
3	0.04279	0.00664	16.2
3 (T 3 shunted)	0.04279	0.00652	16.4

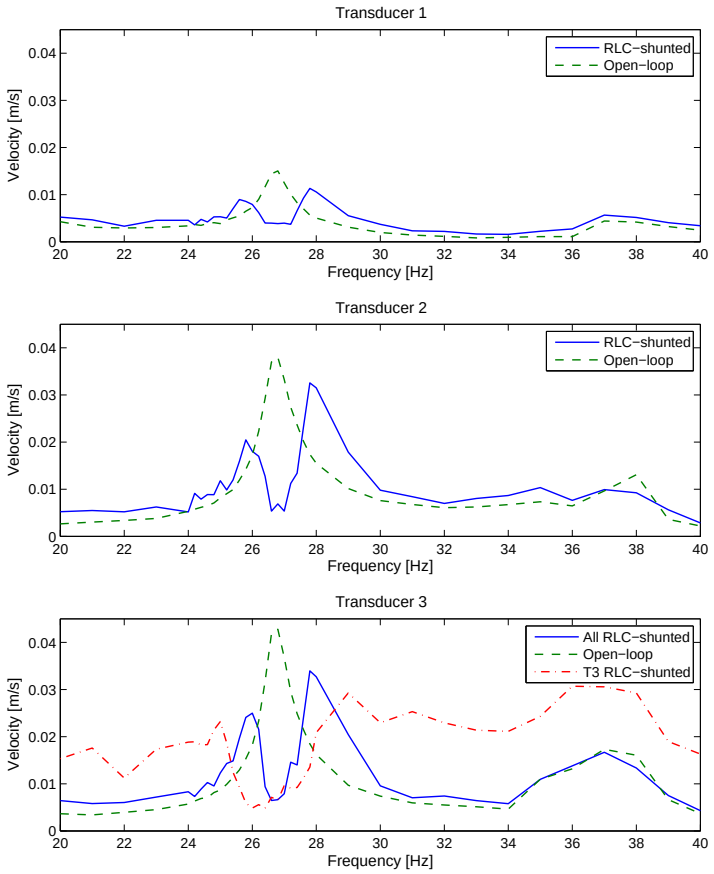

Figure 5.9: Top plate velocities when all transducers are RLC-shunted, measured at the transducers.

5.4 Conclusion

When the RC-controller and the RLC-controller are compared with each other, it can be concluded that RLC-controller has higher resonance peak reduction (Table 5.3). The RC-controller has better performance in regard to the vibration isolation problem: with the RC-controller the transfer between base and top plate does not show peaks around resonance whereas the RLC-controller transfer does show peaks because of the narrow bandwidth. The disadvantage with RC-shunt is that the transfer has a decrease in attenuation at high frequencies. This effect is not seen with the RLC-shunt when all transducers are shunted.

Because of its narrow bandwidth the RLC-controller may prove useful in a multimode system. One is then able to use the RLC-controller to dampen individual modes without affecting other modes.

Table 5.3: Comparison between RC-controller and RLC-controller in resonance peak reduction.

Transducer	**RC-shunt [dB]**	**RLC-shunt [dB]**
1	7.1	11.9
2	6.0	16.2
3	8.3	16.2
3 (T 3 shunted)	11.8	16.4

6

Conclusion

6.1 Conclusions

The end result of this project is a vibration cancellation system consisting of two plates of which the top plate is controlled using a shunt impedance controller. It can be concluded that an RC-controller can provide damping of a resonance peak. The damping that can be achieved depends on the location of the measurement. A peak reduction of 12.1 dB was seen at the centre of the top plate while all three control transducers were powered. When measuring at a control transducer, a reduction of 8.3 dB was found. In case of the RLC-controller, the peak reduction at a control transducer was 16.2 dB while all three transducers are controlling. It was seen that the RC-controller has a large bandwidth and therefore a relatively large frequency range around which the controller operates. This suffices for vibration isolation, but not for multimode damping. Multimode damping requires the controller to operate at a single mode of vibration and therefore requires the controller to be very selective, i.e. have a small bandwidth. This was achieved by the RLC-controller.

Three control transducers are controlling the vibration at a different location on the same plate as three SISO systems. Therefore, all control transducers are completely ignorant to what the others are doing. This means that there will be coupling between the control action of one transducer and the effect on the top plate at a different transducer.

The usage of a synthetic impedance as opposed to a physical shunt network has a big advantage regarding the versatility of the controllers. The controller can be tuned to a specific frequency very easily and a different type of controller is implemented very quickly.

The self sensing principle to measure the back-emf generated by the transducers as a result of vibrations seems to give a valid measurement in case of transducer 2 and 3. However, transducer 1 shows an error of 100 %, which means that this measurement nor the control action based on this measurement can be considered valid.

6.2 Reconsiderations & Recommendations

Although the goal of cancelling vibrations in the top plate was met, some aspects with respect to the system design are reconsidered. Also, there are a number of things that should be considered when continuing work on this project.

- The distributed parameter model of the system was found to be competent up to a frequency of 76.3 Hz. Also, because only one mode of vibration was to be cancelled, a lumped parameter model describing that mode was made. When multimode damping is considered, the models presented in this thesis are not valid anymore. This means that a new model incorporating the desired modes should be made.
- In this sytem, the mechanical parameters of the transducers were assumed to be identical. For a more accurate model, the specific mechanical parameters should be measured and taken into account in the system model.
- The top plate is supported by three control transducers. This ensures that the degrees of freedom of the top plate are not overconstrained. It appeared that this was not very convenient from a modeling point of view, as the symmetry in the system was lost. Therefore, one control transducer needs to support a higher load than the other two. This may have caused the distinct measurements seen in Chapter 5 that often do not resemble the measurements at the other two transducers.
- The RC-shunt parameters are calculated at a specific resonance frequency and by H2-optimisation. This results in a shunt capacitance and resistance. However, some of the RLC-shunt parameters can be chosen freely e.g. the resistance to choose a bandwidth which is given by $\frac{R}{L}$. Because of this, there is no point in an optimisation strategy to find the optimal resistance, as this changes the bandwidth of the controller again. Choosing the optimal parameters is something to look into when continuing this project.
- A different method to measure the back-emf voltage may be considered, as the measurement at transducer 1 did not provide a valid result.
- When the goal is to control the top plate velocity with respect to the fixed world, control on the top plate itself should be considered as opposed to controlling the difference between the top and base plate.
- Two controllers have been evaluated during this project: the RC-shunt and RLC-shunt controllers. Although these controllers showed an acceptable performance, a different kind of controller can be considered, e.g. Impedance Synthesis or Ideal Controller [4].
- In practice it was expected that the system cannot be treated as three independent SISO systems since the output of each SISO system will influence the output of another SISO system. An improvement would be to treat the system as a MIMO system instead of three SISO systems. The coupling between the transducers can then be taken into account and a better control performance may be seen.

Appendix A

Transducer Characterisation

The transducer used in this project is quite similar in structure to a normal loudspeaker (refer to Figure 2.1). It consists of a coil which produces a magnetic field when a current is fed through. This will move the core magnet which is mounted inside the coil and supported by a flexible structure.

Because a transducer converts energy from one domain into another, in this case the mechanical and electrical domains, care was taken that during measurements this energy transfer was minimised. This was done by either constraining the mechanical translation during measurements at the electrical port and having open terminals at the electrical port while doing measurements at the mechanical port. While measuring the coupling between these two domains no restrictions were applied.

A.1 Spring Constant

The spring constant of the transducer was determined by putting a weight on the core and then measuring the deflection of the core with respect to the housing. The spring constant was calculated for three different weights using Equation A.1 and then averaged.

$$F = -k \cdot x \tag{A.1}$$

Table A.1 lists the measurement.

Table A.1: Transducer spring constant measurement by placing a weight on the core and measuring the deflection.

Load [N]	**Deflection [m]**	**Spring constant [N/m]**
1.447	$80{\cdot}10^{-6}$	18087.19
2.894	$150{\cdot}10^{-6}$	19293.00
4.341	$220{\cdot}10^{-6}$	19731.48

The average of these measured spring constants is 19037.22 N/m.

A.2 Resonance Frequency

The resonance frequency of the transducer was determined by putting a sinusoidal input voltage at the terminals of the transducer and then measuring the acceleration of the core. At the resonance frequency the deflection of the core will be maximum, so then the acceleration will also be maximum. The acceleration was measured using a PCB Piezotronics 353B17 accelerometer. The maximum acceleration was found at 38.63 Hz.[1] Because damping is present in the system, this frequency is the damped resonance frequency ω_d. The damped resonance frequency is related to the resonance frequency by:

$$\omega_d = \omega_c \cdot \sqrt{1-\zeta^2} \tag{A.2}$$

where ζ is the damping ratio of the transducer (see Section A.4). Thus the resonance frequency is:

$$\omega_c = \frac{\omega_d}{\sqrt{1-\zeta^2}} = \frac{38.63 \cdot 2\pi}{\sqrt{1-0.0339^2}} = 242.86 \text{ rad/s} = 38.65 \text{ Hz} \approx \omega_d \tag{A.3}$$

A.3 Core Mass

The mass of the core was determined by relating it to the resonance frequency and the spring constant:

$$\omega_c^2 = \frac{k}{m} \tag{A.4}$$

$$m = \frac{k}{\omega_c^2} = \frac{19037.22}{2\pi \cdot 38.65^2} = 0.323 \text{ kg} \tag{A.5}$$

A.4 Damping Coefficient

The damping coefficient of a mass-spring-damper system is given by:

$$d = 2\zeta\sqrt{k \cdot m} \tag{A.6}$$

where ζ is the damping ratio of the system, k is the spring constant and m is the vibrating mass. If the system is underdamped, the damping ratio is given by:

$$\zeta = \frac{1}{\sqrt{1+\left(\frac{2\pi}{\delta}\right)^2}} \tag{A.7}$$

where δ represents the logarithmic decrement. The logarithmic decrement is used to describe two successive peaks in an underdamped oscillation:

$$\delta = \frac{1}{n} ln\left(\frac{x_0}{x_n}\right) \tag{A.8}$$

where x_0 is the greater of the two peaks and x_n is the amplitude of a peak n periods away. Figure A.1 illustrates this concept.

[1] The transducer was mounted on an MDF plate of 50 by 60 cm which may have influenced the resonance frequency measurement. Ideally, the transducer should be fixed to a heavy solid object, e.g. a concrete block, as to minimise this influence.

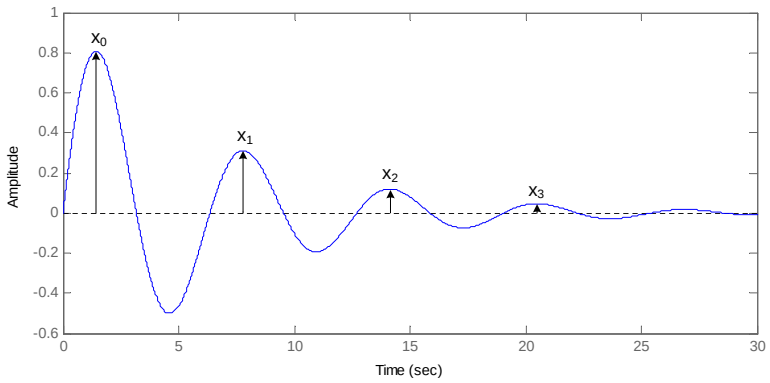

Figure A.1: Example of an underdamped oscillation where the peaks used for calculating the logarithmic decrement are indicated.

For this measurement, two transducers were mounted on an MDF plate about 20 cm apart. One transducer was actuated by a sinusoidal voltage, the acceleration of the other transducer as a result of the propagation of vibration through the MDF plate was measured by an accelerometer. After stopping the actuation, the accelerometer showed an underdamped oscillation. The amplitude of four oscillation peaks was measured (see Table A.2), so three values for the logarithmic decrement with respect to x_0 were found using Equation A.8.

Table A.2: Logarithmic decrement measurement of the underdamped oscillation of the transducer.

Peak	**Amplitude [V]**	$\boldsymbol{\delta}$
x_0	2.563	-
x_1	2.031	0.2327
x_2	1.688	0.2088
x_3	1.406	0.1978

The average value of the logarithmic decrement, δ_{avg} =0.2131, was used in calculating the damping ratio by filling in Equation A.7:

$$\zeta = \frac{1}{\sqrt{1 + \left(\frac{2\pi}{0.2131}\right)^2}} = 0.0339. \tag{A.9}$$

The damping coefficient was found using Equation A.6:

$$d = 2 \cdot 0.0339\sqrt{19037.22 \cdot 0.323} = 5.32 \text{ Ns/m}. \tag{A.10}$$

A.5 Coupling Coefficients C_{iF} and C_{vV}

The force $F_s(t)$ exerted by the coil on the core is related to the supplied current i(t) by:

$$F_s(t) = B \cdot l \cdot i(t) \tag{A.11}$$

where B is the magnetic field strength expressed in T or Wb/m^2 and l is the length of the current carying wire. Equation A.11 is often written as:

$$F_s(t) = C_{iF} \cdot i(t) \tag{A.12}$$

where C_{iF} is defined as the coupling coefficient between the current through the coil and the force exerted on the core. Similarly, when the core is moved with a velocity v with respect to the coil, a voltage V will be induced at the terminals of the transducer:

$$V(t) = B \cdot l \cdot v(t) = C_{vV} \cdot v(t) \tag{A.13}$$

where C_{vV} is defined as the coupling coefficient between the velocity of the core and the voltage induced in the coil. These coupling coefficients were assumed to be equal, but are not identical for all control transducers and are *not* constant over frequency.[2] These coefficients were measured for all three control transducers by exciting the disturbance transducer at 26.9 Hz to cause vibration in the control transducers. The velocity of the core with respect to the housing of the transducer is determined by two accelerometers. One is placed on the top plate, the other on the housing of the transducer. By assuming a sinusoidal movement $x(t)$ of the core, the velocity can be determined by the accelerometer measurement.

$$\begin{aligned} x(t) &= A \cdot sin(\omega t) \\ \dot{x}(t) &= A\omega \cdot cos(\omega t) \\ \ddot{x}(t) &= -A\omega^2 \cdot sin(\omega t) \end{aligned} \tag{A.14}$$

The maximum velocity is then given by:

$$\dot{x}_{max}(t) = \frac{\ddot{x}_{max}(t)}{\omega} \tag{A.15}$$

The induced voltage by the transducer is measured at its terminals. This voltage divided by the velocity results in the coupling coefficient between the electrical and mechanical domain, i.e.:

$$C_{vV} = \frac{V(t)}{v(t)}. \tag{A.16}$$

Table A.3 lists the calculated coupling coefficients and the average value per transducer at a disturbance frequency of 26.9 Hz.
It is noted that the difference between the value of transducer 1 and transducer 3 is 80 % which justifies the usage of specific coupling coefficients instead of a universal value.

[2] During measurements with control transducer 1 at 36.8 Hz and 76.3 Hz, the coupling coefficient changed by a factor three.

Table A.3: Calculated control transducer coupling coefficients C_{vV} and average values at 26.9 Hz.

	Transducer 1	**Transducer 2**	**Transducer 3**
Measurement 1	2.1186	3.6294	3.7400
Measurement 2	2.0541	3.6427	3.6832
Measurement 3	1.9842	3.6360	3.6756
Average	2.0523	3.6361	3.6996

A.6 Electrical Impedance, Inductance and Resistance

The electrical impedance was modeled as an inductance in series with the coil resistance as seen in Figure 2.1b. These parameters are not identical for the three control transducers and are also not constant over frequency. A Philips PM 6304 RCL-meter was used to measure the inductance and series resistance. While doing these measurements, the translation of the transducer core was constrained as to prevent movement and therefore influence on the measurement.

The RCL-meter is able to measure at various frequencies from 50 Hz up to 100 kHz. The measurements were done at 50 Hz which is the frequency closest to 26.9 Hz. The electrical impedance was calculated using the inductance and resistance values, i.e.:

$$|Z_i| = \sqrt{R_i^2 + (\omega L_i)^2}. \tag{A.17}$$

Table A.4 lists the inductance and resistance values measured by the RCL-meter as well as the impedance value calculated according to Equation A.17.

Table A.4: Measured inductance and series resistance from which the transducer impedance was calculated.

	Symbol	**Transducer 1**	**Transducer 2**	**Transducer 3**
Resistance	R_i [Ω]	3.6133	3.7166	3.8396
Inductance	L_i [μH]	518	533	597
Impedance	Z_i [Ω]	3.6170	3.7204	3.8442

It can be seen that the difference between the resistance of transducer 1 and transducer 3 is more than 6 %, while the difference between the inductance is more than 15 %, not taking into account the measurement error. The measurement error for the resistance is given by:

$$R'_e = (R_e \pm \Delta R_e)(1 \pm \Delta R_{e\%}) \pm 1 \text{ digit} \tag{A.18}$$

where R'_e is the measured resistance, R_e the true resistance, ΔR_e the repeatability error, $\Delta R_{e\%}$ the error limit in percentages and '1 digit' a constant error term depending on the measurement range of the RCL-meter. Equation A.18 also holds for the error in the inductance measurement; R should then be substituted by L.

The error limits were found in the Philips PM6304 manual [7] and are listed in Table A.5.

Table A.5: Error limits for the resistance and inductance measurements at 50 Hz.

	Resistance	**Inductance**
Repeatability	0.1 Ω	1 μH
Error limit	0.2 % at 4 Ω	3 % at 500 μH
Error constant (1 digit)	0.0001 Ω	1 μH

Using the values from Table A.5 lower and upper bounds for the resistance and inductance values in Table A.4 can be calculated. The error between the lower bound value of transducer 1 and upper bound value of transducer 3, i.e. a worst case error scenario, then increases to more than 12 % for the resistance and more than 23 % for the inductance. As a result, the error between the impedance values is more than 12 % which directly affects the self-sensing calculation used for estimating the transducer voltage. Obviously, the more accurate this estimation is, the better the control performance will be. This again justifies the usage of specific values for the three control transducers.

Appendix B

Schematics

Figure B.1 shows the electrical schematic of the interface circuit which is used to power the transducer and to measure the transducer and measurement resistor voltages in dSpace. Three identical circuits were built as three transducers are used for control. To power the circuit a symmetrical 15 V power supply is used. For a list of the component types and values, refer to Table B.1. The measurement resistor is specific for each circuit. See Section 4.3.2 for the accurate values.

Component	**Type/Value**	**Usage**
U_1	OPA548	Heatsinked power opamp
U_2, U_3	uA741	Generic opamp
R_1, R_7	1 kΩ	1591 Hz LPF
R_2	1 kΩ	Power opamp 4.8 A current limiter [8]
R_3 to R_6, R_8 to R_{11}	12 kΩ	Unity gain differential amplifier
C_1, C_4	100 nF	1591 Hz LPF
C_2, C_3, C_5	100 nF	IC decoupling capacitors
C_6, C_7	100 μF	Power supply buffering
Z_L	-	Load impedance, i.e. the transducer
R_m	1 Ω	Measurement resistor

Table B.1: Component types and values used in the interface circuit of Figure B.1

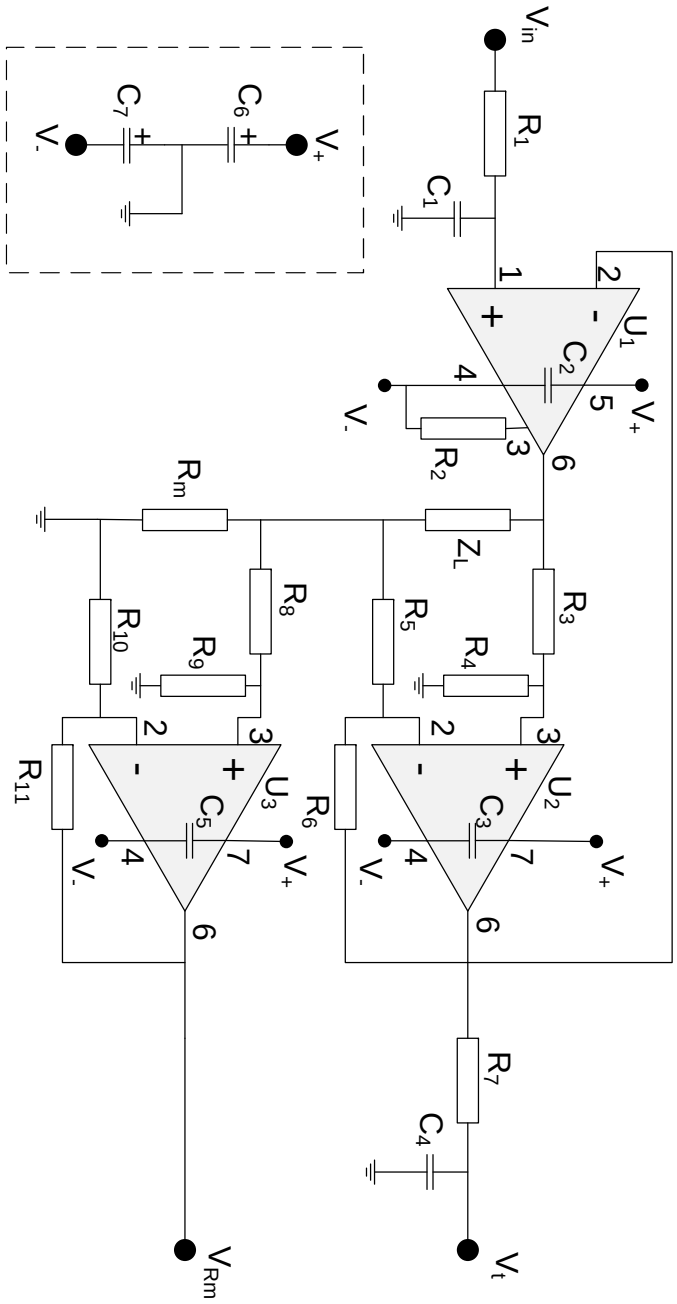

Figure B.1: Electrical schematic of the interface circuit.

Appendix C

Quick Reference Manual

This quick reference manual describes the main features and operating procedure of the vibration cancellation system.

C.1 Features

The system consists of two plates: a base plate to which four electromagnetic transducers are mounted and a top plate that rests on three of those transducers. The vibration in the top plate at 26.9 Hz is cancelled by those three control transducers. The fourth disturbance transducer is used to induce vibrations in the base plate which will vibrate the top plate.

C.1.1 Disturbance transducer

The disturbance transducer is powered by a 50 W JayCar amplifier seen in Figure C.1.

Figure C.1: The JayCar amplifier used to power the disturbance transducer.

The input should be a sinusoidal signal (typically 26.9 Hz) at 250 mV peak to peak voltage, which is often generated by a waveform generator (e.g. Agilent 33250A). *Ensure that the output impedance of the waveform generator is set to High-Z instead of 50* Ω. The input voltage can be increased to 500 mV peak to peak for a short period of time, to induce greater vibrations. A symmetrical 15 V power supply is used for this amplifier. The red lead indicates +15 V, the yellow -15 V and the black lead indicates the ground connection. At an input of 250 mV peak to peak, the dissipated power is 6.6 W_{RMS}.

C.1.2 Control transducer

Each control transducer is powered by an identical circuit as shown in Figure C.2.

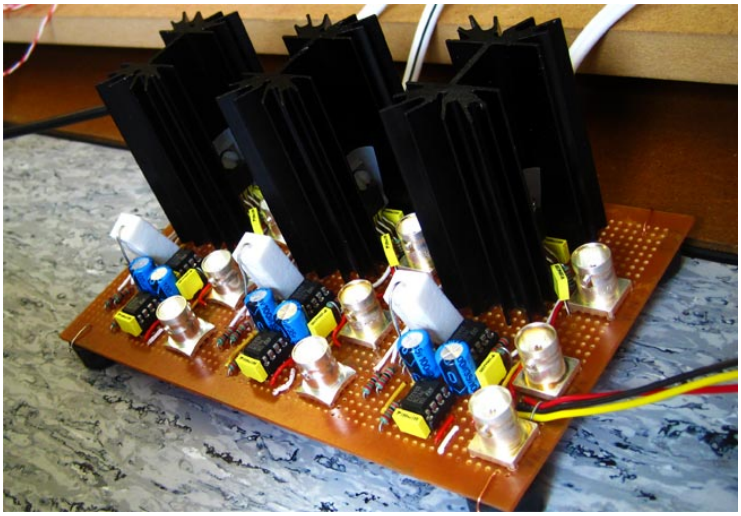

Figure C.2: The interface circuits used to power the control transducer and provide the transducer and measurement resistor voltages.

These three circuits are all mounted on a single board and are labeled indicating which circuit should be used for a particular transducer. Each circuit features three connections: an input V_{in} (right BNC connector closest to the heatsink) which should be connected to the control signal output coming from dSpace, an output V_t (middle BNC connector) which represents the voltage across the transducer and an output V_{Rm} (left BNC connector) which represents the voltage across the measurement resistor used to calculate the current flowing through the transducers. These two measurements are needed to calculate the back-emf voltage generated by the transducers as a result of mechanical vibrations. Again, a symmetrical 15 V power supply is used for these amplifiers using the same coloured leads as the disturbance transducer amplifier. The maximum power dissipation when all three transducers are powered is 12 W.

When using this circuit, beware of the following:

- Do not float any of the inputs V_{in} as these inputs are not pulled down. If no input is connected, a random signal will be the reference which may cause overheating of the power opamp or measurement resistor.

- Do not turn on the power supply to these interface circuits when it is not properly connected and no control signal is offered.

C.1.3 dSpace

When the MATLAB Simulink model is simulated externally, it is run by the onboard digital signal processor found on the dSpace DS1103 Controller Board. This board acquires the two measurement signals per circuit (so six in total) using 16-bit AD converters, calculates the back-emf voltage V_{emf} and a control signal as reference output. This output is fed to the input of the interface circuit V_{in} by a 14-bit DA converter. Table C.1 lists all converter ports used per circuit and can be used as a wiring diagram. The transfer functions implemented in the MATLAB Simulink model are given in Equation 4.3 and 4.4.

Table C.1: AD and DA converters on the dSpace DS1103 used for signal acquisition and reference voltage output.

Signal	**Symbol**	**Circuit 1**	**Circuit 2**	**Circuit 3**
Reference voltage	V_{in}	DACH1	DACH3	DACH5
Transducer voltage	V_t	ADCH1	ADCH7	ADCH13
Measurement resistor voltage	V_{Rm}	ADCH3	ADCH9	ADCH15

C.2 Operation

A couple of simple steps have to be followed to ensure a properly functioning system.

- Connect the disturbance amplifier to the disturbance transducer (the two wires can be connected either way) and to the symmetrical 15 V power supply (red lead = +15 V, yellow lead = -15 V, black lead = ground). Do not set the current limiter below 1.0 A as a couple of hundred mA are needed to drive the transducer. Do not turn on the power supply yet. Connect the amplifier to the waveform generator.

- Set the waveform generator at a sinusoidal output of 26.9 Hz and 250 mV peak to peak, while ensuring that a High-Z output impedance instead of 50 Ω is selected. Enable the output of the generator.

- Connect the interface circuits to the correct transducers. Each circuit and transducer is labeled, so make sure that the correct transducer is connected to the correct circuit. Connect all BNC connections on the interface circuits with the AD and DA ports on the dSpace controller board. Refer to Table C.1 for a wiring diagram. Connect the interface circuits to a 15 V symmetrical power supply (again the red lead = +15 V, yellow lead = -15 V and black lead = ground). This power supply can be the same as the one for the disturbance amplifier, but make sure that enough current can be provided to run them both. Do not turn on the power supply yet.

- Start MATLAB Simulink and the dSpace Control Desk and open the correct Simulink model. Choose the option 'external' in Simulink and press CTRL-B to build the model. After a while, the model is built and is run by the dSpace controller board.
- Turn on the power supply to the disturbance amplifier and watch the system vibrate.
- Turn on the power supply to the interface circuits to enable control of the top plate. Vibrations will be reduced visibly.

References

[1] MacMartin, D. G., *Collocated structural control: motivation and methodology*, Proceedings of the IEEE International Conference on Control Applications, p. 1092-1097, September 1995

[2] Gawronski, W. K., *Advanced Structural Dynamics and Active Control of Structures*, Springer, 2004

[3] Behrens, S., *Passive and Semi-active Vibration Control of Piezoelectric Laminates*, MSc. thesis, The University of Newcastle, Australia, December 2000

[4] Behrens, S., *Vibration Control using Shunted Piezoelectric and Electromagnetic Transducers*, PhD thesis, The University of Newcastle, Australia, May 2004

[5] Meirovitch, L., *Fundamentals of Vibrations*, McGraw-Hill Higher Education, p. 345-346, International Edition 2001

[6] Hanson, B., Levesley, M., *Self-sensing applications for electromagnetic actuators*, Science Direct, Sensors and Actuators A 116 (2004) 345-351, June 2004

[7] *Philips PM 6304 PROGRAMMABLE AUTOMATIC RCL METER*, Reference Manual, 1993

[8] *Texas Instruments OPA548 Operational Amplifier*, Datasheet, October 2003